

Materials Analysis And Research Laboratory

FROST ACTION IN ROCKS AND CONCRETE

**FINAL REPORT
APRIL 30, 1986**

**IOWA DOT PROJECT HR-258
ERI PROJECT 1648**

Sponsored by the Highway Division of the
Iowa Department of Transportation and the
Iowa Highway Research Board.

ENGINEERING RESEARCH INSTITUTE

iowa state university

eri 86-445

B. V. Enüstün
B. Gunnink
W. Dubberke
T. Demirel

FINAL REPORT

FROST ACTION IN ROCKS AND CONCRETES

"The opinions, findings, and conclusions expressed in this publication are those of the author and not necessarily those of the Highway Division of the Iowa Department of Transportation."

Iowa DOT Project HR-258
ERI Project 1648
ISU-ERI 86-445

Sponsored by the Iowa
Department of Transportation,
Highway Division and Iowa
Highway Research Board.

Table of Contents

	Page
Introduction.....	1
Part 1. Frost Pressure.....	2
Part 2. Ice Porosimeter.....	6
Oscillator Circuitry.....	7
Microcomputer.....	8
Eight-Bit Digital to Analog Converter.....	8
Experimental Procedure.....	8
Part 3. Rate of Ice Growth.....	14
Part 4. Overview of Frost Action on Rocks and Concretes.....	20
Conclusions.....	27
Figures 1 through 26	29-54
Appendix I	55

FINAL REPORT

FROST ACTION IN CONCRETES AND ROCKS

Introduction

The objectives of the project were to develop methodologies for (i) prediction and measurement of the magnitude of pressure which develops within pores of saturated porous materials upon freezing, (ii) determination of pore structure (pore size distribution) of porous materials; (iii) prediction and measurement of the rate with which pore ice grows; and (iv) prediction of frost susceptibility of porous materials with varying pore structures.

As with all research endeavors solution of one problem leads to another one and this project was no exception. Emergence of new problems and the measures taken as the work progressed were discussed in progress reports submitted to the board. This final report will discuss only the conclusive finds and suggest measures to be taken for future investigations. The theory discussed in the proposal is not repeated in this report for the sake of brevity. However, the paper published as part of this project containing the theory is attached as Appendix I for the reader interested in the theory. In conformity with the objectives, this report consists of four parts.

In accordance with the project contract two ice (or phase transition*) porosimeters** were built and one will be delivered to the Iowa DOT after training of a DOT technician under the supervision of Mr. Wendell Dubberke with assistance from ISU researchers. During the training period debugging and further improvements in software will continue.

* The term phase transition is a more general term and better represents the instrument.

**U.S. Patent No. 4,453,398, issued to ISU Research Foundation on June 12, 1984.

Part 1. Frost Pressure

For studying the expansive pressure of a growing ice lens a two-piece pressure cell was designed and made in stainless steel as shown in Figure 1 after the various modifications as discussed in the progress reports. To conduct an experiment the cell is filled with helium gas under a constant pressure measured by the pressure transducer connected directly to the gas line. A thin layer of ice is allowed to form at the lower base of the saturated porous sample in the pressure cell. The glass capillary tubing filled with water and connected to the water-filled upper section of the sample holder is used to detect the flow of water through the sample by observing the movement of the water level in the capillary. This device is used as a null indicator. The gas pressure adjusted to keep the water level steady should be equal to the equilibrium ice pressure at the set sub-zero temperature.

Using the modified apparatus filled with helium gas for studying the expansive pressure of a growing ice lens as a function of temperature, considerable effort was made to explore and establish operating conditions to obtain reproducible measurements.

A further development was also made on the apparatus to monitor the water flow through the porous sample electronically instead of by visual observation. It consisted of wrapping two 1 cm wide aluminum sheet strips around the glass capillary tube of the flow-meter. The spacing between those strips was about 3 cm. As the water meniscus travelled within this space up or down, the capacitance between the aluminum sheets varied accordingly. After calibration, the capacitance measured by a capacitance bridge and recorded by a strip chart recorder could measure the water level. Thus, it was possible to determine the rate of flow using the recorded data at a given temperature and pressure. The complete experimental assembly is shown in Fig. 2.

Two problems were encountered in the final phase of this study as described below:

(1) The transducer used for pressure measurements did not stand the occasional fast pressure changes and failed in an early stage. It was replaced by a conventional mechanical pressure gauge reading up to 1000 PSI and graduated in 10 PSI.

(2) At higher pressures, helium gas dissolved in pore water and found its way, diffusing through Vycor, into the bulkwater above it during prolonged experiments. Of course, this upset the flow rate measurements. This difficulty was overcome by allowing a fast downward flow for several hours by lowering the helium pressure to 30 PSIA and the bath temperature to -10°C before each measurement. This way it was possible to create a helium-free pore water zone in the uppermost section of the porous material, at least for a few hours to take reliable measurements, until rediffusion of helium began to interfere with these measurements. A typical set of recorded data on capacitance versus time is shown in Fig. 3. The initial straight section of this plot indicates a slow downward flow. It is followed by a fast unsteady upward movement of the meniscus, indicating formation of helium bubbles. (For future studies it is recommendable to seal the lower end of the porous material with a layer of mercury to prevent its contact with the gas in the pressure cell.)

The procedure to take a flow rate measurement was as follows: setting the gas pressure slightly above atmospheric, the bath temperature was raised a few degrees above zero for a few minutes to melt a thick layer of ice which might have built up at the base of the porous sample and possibly retarded transmittance of pressure. Then, the temperature was lowered to -10°C for several hours to reform ice and depress dissolved helium as mentioned above.

The water level in the flow-meter was adjusted to be between the aluminum electrodes. The required pressure and temperature were then set and the flow was recorded as described above until a steady flow rate was established for about one hour. This stage was reached in 1-2 hours. The pressure and temperature settings were so chosen to obtain extremely slow downward or upward flow in order to interpolate the results to zero rate with reasonable certainty, as will be discussed below.

The results obtained with Vycor used as porous material are tabulated in Table 1, assigning + sign to downward, - sign to upward flow, and plotted in Fig. 4.

At atmospheric ice pressure small rates were found to be controlled by hydraulic permeability of the porous medium varying almost linearly with temperature in the vicinity of zero rate as shown in Figures 5 and 6. (These figures will be discussed in Part 3 of this report). It is reasonable to assume that the same trend holds at higher ice pressures. On this assumption, the measured rates at each constant ice pressure were interpolated to zero rate by linear regression to determine the equilibrium temperature as shown in Fig. 4. The equilibrium temperatures estimated this way at various pressures are given in Table 2. Finally, in Fig. 7 the expansive gauge pressure is plotted against experimentally determined equilibrium temperature.

Table 1. Rate of flow of pore-water through Vycor (in 1.4 mm bore flow-meter) toward pressurized ice phase at various pressures and temperatures.

<u>Ice Pressure PSIA</u>	<u>Expansive Pressure Atm. (gauge)</u>	<u>Temperature C</u>	<u>Rate of flow mm/h</u>
200	12.6	-2.72	+0.38
200	12.6	-2.44	+0.36
200	12.6	-0.85	-0.095
350	22.8	-2.31	+0.053
350	22.8	-2.00	0
350	22.8	-1.92	-0.030
500	33.0	-3.03	+0.064
500	33.0	-2.64	-0.095
700	46.6	-4.03	+0.014
700	46.6	-3.76	+0.019
700	46.6	-3.55	-0.017
900	60.2	-5.39	+0.200
900	60.2	-5.00	+0.020
900	60.2	-4.72	-0.045

Table 2. Experimentally determined equilibrium temperatures at various heaving pressures.

<u>Expansive pressure, atm. (gauge)</u>	<u>Equilibrium temperature, C</u>
12.6	-1.19
22.8	-2.04
33.0	-2.87
46.6	-3.69
60.2	-4.88

Substituting $p_w = 0$ for pore water gauge pressure, and appropriate numerical values for ρ_i , λ and T_0 of Eq. (1) in the Project Proposal, $p_i = \rho_i p_w / \rho_w + \rho_i \lambda (-t) / T_0$, the theoretical relationship between expansive pressure in atmosphere and temperature in centigrade can be obtained as

$$p_i = 11.0 (-t)$$

This equation is represented in Fig. 7 by a dashed line. It will be seen that the experimental results agree with the theory perfectly down to a temperature of -2.5°C . Beyond that point, however, the experimental pressures are somewhat larger than the theoretical. It was not possible to resolve whether this deviation was due to a systematic experimental error or a real physical effect. In either case, as the experimental points beyond -3.5°C run parallel to the theoretical line, the theoretical equation appears to predict the expansive pressure satisfactorily from the practical point of view.

Part 2. Ice Porosimeter

The ice porosimeter developed within the project, which proved to be superior to mercury porosimeter, consists of a cryostat, a dilatometer, a variable mercury-aluminum capacitor, a thermistor, a measuring circuitry, a microcomputer and a plotter. The dilatometer shown in Fig. 8 is made of Lexan and is equipped with volume and temperature sensors. The rest of the ice porosimeter is built around the dilatometer. The cryostat used was a Haake model A82, suitable to maintain constant temperature above -40°C to within $\pm 0.01^\circ\text{C}$. To measure volume change i.e. the level of mercury inside the capillary stem a variable "mercury-aluminum" capacitor was used as part of a square wave oscillator. The oscillator's output frequency varies with corresponding changes in the value of the 'mercury-aluminum' capacitor. It is

then a trivial matter to have a computer measure the period of a square wave. This method has the advantage that the circuitry is very simple, and hence, inexpensive. Furthermore, because of the circuit's simplicity, there is less error introduced into the data. The tungsten wire inserted into the dilatometer provides the electrical contact to the mercury.

A thermistor (model SP85DA102FA1) manufactured by Thermometrics, Edison, NJ, was used to measure the temperature of the area surrounding the sample. The dead-end glass inlet that houses the thermistor is near the top of the inside of the dilatometer to prevent samples from floating to the top. This also assures that the temperature being measured is representative of the temperature of the sample. A drop of kerosene in the housing aids in conduction of heat between the thermistor and the sample. The method used to measure the resistance of the thermistor is virtually identical to that for measuring the capacitance of the 'mercury-aluminum' capacitor. The thermistor is part of a square wave oscillator that varies its output frequency with changes in the thermistor's resistance.

Oscillator Circuitry. The two oscillators used (Fig. 9) are virtually identical. The heart of these circuits is a CMOS (Complimentary Metal Oxide Semiconductor) ICM7556 timer chip, manufactured by Intersil, and operates as a simple astable multivibrator. The capacitance of the 'mercury-aluminum' capacitor varies from 3 to 35 pico-farads. Such small capacitances would normally cause the circuit to generate a very high frequency; too high for the computer to measure. To lower the frequency, fixed timing resistors with very high resistances (22 meg-ohms and 44 meg-ohms) were used. A CMOS timer chip was used, because such large resistances limit the circuit's current to a level that

is too low for a standard 556 timer chip to be used. A further advantage of this circuit is that the output frequency is independent of moderate fluctuations in the supply voltage.

Microcomputer. The computer used is an Apple IIe personal computer with 128K bytes of memory, and special I/O (Input/Output) cards from John Bell Engineering. These cards are liaisons between the Apple IIe, and the dilatometer-cryostat combination. They have two 6522 parallel I/O chips, each of which have two 16-bit timer-counters, two 8-bit I/O ports, and four separate I/O lines.

Eight-Bit Digital to Analog Convertor. The software program, MASTER CONTROL, that runs on an Apple II computer controls the temperature of the cryostat by loading a number in the range of 0 to 255, into the I/O card. This number is then output, in binary form, from one of the 8-bit ports on the card. The 8-bit port is connected to a DAC (Digital to Analog Convertor, Figure 10) which then converts the data to a corresponding voltage. The DAC's output voltage is in the range +0.04 to -0.35 volts, which corresponds to +4°C to -35°C. The output of the DAC is connected to an external temperature control socket on the circulator bath. Every ten millivolts applied to this connector corresponds to one degree centigrade. Negative voltages correspond to negative temperatures.

Figure 11 shows a data flow diagram of the porosimeter, including hardware and software. Shown are the functional blocks (rectangles), and the data or information (arrows) that is passed between the functional blocks.

Experimental Procedure. The porous sample to be studied is saturated with water by a suitable method such as capillary suction, vacuum saturation, steam

saturation, etc. and placed in the dilatometer cup. At that stage it must be visibly wet and surrounded by a film of excess liquid. Powdered samples may be introduced into the dilatometer in the form of pastes enclosed in suitable containers. The dilatometer is assembled and filled with mercury through the inlet so that the mercury level reaches the lower end of the stem. The assembly is immersed in the cryostat maintained at a few degrees above 0°C up to the lower end of the air outlet tube. When thermal equilibrium is established, the mercury level is reset and the test is initiated by turning the control over to the computer.

Developments in ice porosimetry continued during the final phase of the project in the following directions:

(1) Minor modifications were made in the design of Lexan dilatometer such as (a) reducing the wall-thickness of its body by a factor of two to promote heat conduction for faster thermal equilibration, (b) joining the mercury inlet with the graduated stem to eliminate one glass-to-Lexan connection and (c) short-circuiting the mercury to the stainless steel handle to simplify the construction of mercury contact, thus to use the handle as a connection post. A second Lexan dilatometer so designed was made by the machine shop and put into operation.

(2) The electronic noise showing some periodicity along the temperature axis experienced in the output of the volume measuring interface introduced some uncertainty in the small pore-size-range. The smoothing routine in the software could take care of this problem if phase transition signals in this range were large enough to tolerate noise, as in the case with the Vycor studied earlier. However, in testing samples of rocks which do not contain many pores in this range, even the routine smoothing could not solve the problem. Considerable time was devoted to diagnose the source of this noise systematically. It was

ultimately traced to a resonating interaction between the volume and the temperature measuring interfacing circuits which were housed in the same box and the network of running cables. This problem in the hardware was solved by reconstructing the two circuits physically separated from each other. To process the noisy data of already run experiments, a new smoothing routine was developed and introduced into the software.

(3) Another source of error discovered in evaluating the raw data was the assumption of linear thermal expansion of the dilatometer material. Measurements taken by filling the Lexan dilatometer with mercury only, showed a slight non-linear component, in contrast to the previous case of glass dilatometers. To take care of this non-linearity, revisions were made in the data processing method and software. The revised method calls for a computerized correction of raw volume versus temperature data, using a 2-parameter quadratic function which is characteristic for the dilatometer used.

The results of ice-porosimetric and mercury porosimetric tests run in our laboratory on a Vycor sample were compared and it was concluded that mercury intrusion data, obtained with a Quantachrome instrument, which agree with ice-porosimetric cooling data, measure the pore-neck size; while mercury extrusion data are not correlated to any characteristic pore size in the present state of the art. Mercury porosimetric tests repeated on the same sample with a Micromeritics instrument by the manufacturers of this equipment confirmed this conclusion beyond any doubt. In Fig. 12 we compare the ice-porosimetric neck-size and body-size distributions with the new mercury intrusion and extrusion data, respectively. Note the remarkable agreement between ice-porosimetric neck-size (cooling) and mercury intrusion data, in contrast to a large disagreement between ice-porosimetric body-size (warming) and mercury extrusion data.

Four of the rock samples prepared and supplied by Mr. W. Dubberke were subjected to ice-porosimetry using the first Lexan dilatometer. Having run a test on the rock sample Ullin, and reported the computer processed results in the Progress Report No. 5, we detected a drift in the calibration of the temperature measuring interface due to replacement of a component prior to the test. The calibration was repeated and the raw data on Ullin were reprocessed accordingly.

The new porosimetric results on this sample as well as on the other three rock samples are presented in Figs. 13-22. It must be repeated at this point that "warming" curves on these plots are related to pore-body size distributions, while "cooling" curves to pore-neck size distributions. It will be noticed that volume versus temperature data on cooling at temperatures very close to 0°C are either lacking or erratic due to supercooled freezing. Reliable cooling data in this range is obtainable only by elimination of supercooling coupled with very slow cooling. The operation software has not yet been perfected to the extent of providing both of these requirements. Since it is this region of the curves that is needed for establishing the size of apparently large pore necks (if any) in the rock samples, only the warming branch of the curves but not the cooling branch were analyzed for size distribution at this stage. However, judging from the available sections of these curves as compared to warming curves, neck and body-size distributions in these samples should not differ greatly from each other. This is also confirmed by a fair agreement between body-size distributions derived from warming data and mercury intrusion data as will be discussed now.

Median pore radii of these samples determined from mercury intrusion data by W. Dubberke are tabulated in the 2nd column of Table 3, and also marked by

vertical dash and dot lines on pore size distribution plots in Figs. 14, 16, 18, 20 and 22. The size distribution curves appear to be compatible with these values, except in the case of Lamont where the amount of very large pores seem to have been underestimated by ice porosimetry. This is because the latter sample contains a large amount of very large pores and, therefore, forces the limits of the method of ice porosimetry. A careful analysis of the warming curve in Fig. 17 reveals that most of the pore-ice has melted slightly above the measured temperature of 0°C , and, therefore, the method could not detect its presence. This means that in the vicinity of this point the thermal equilibrium was not perfect due to a substantial phase transition over a narrow range of temperature, and that for more accurate results the warming rate must be lower than 5°C/hr in this range.

Table 3. Properties of Rock Samples

Sample	Median pore radius by mercury intrusion, \AA	Gravimetric porosity, ml/g	Porosity by ice ml/g	Difference ml/g	Al_2O_3 %	Durability
Lamont	6900	0.042	0.039	0.003	0.27	94-98
Montour Oolite	2200	0.023	0.012	0.011		70-80
Ullin	700	0.022	0.010	0.012	0.70	17
Stanzel 15A	3200	0.037	0.016	0.021	1.13	9

The porosities of these rock samples estimated from computer plotted volume versus temperature curves of warming are given in Table 3 together with porosities determined gravimetrically by the conventional method. The porosities determined by gravimetry and by ice-porosimetry are in good agreement in the case of the first sample. In the case of the other three samples, however, ice porosimetry appears to underestimate porosity significantly. The difference is the largest in Stanzel 15A. After drying at 110°C and resaturating in boiling water for six hours (twice as long as that before) the ice porosimetry test repeated on the very same sample gave a porosity value of 0.008 ml/g which was even smaller than the first result.

In Fig. 22 we compare the pore size distributions of this sample derived from the first and second runs of ice porosimetry. It appears that not only the amount of measurable pore volume, but also the pore size has decreased upon prolonged boiling.

Dubberke's studies on this rock indicate that its performance as concrete aggregate is very poor and it contains a high percentage of evenly distributed clay. Also in Table 3 the difference between gravimetric and ice-porosimetric porosities of all four samples are contrasted to their Al_2O_3 contents, which is a measure of their clay contents, and to the results of durability tests. A correlation is observed between the above defined porosity difference and the clay content as well as the durability performance of these rocks: The greater the difference, the larger is the clay content and the poorer is the performance.

It appears that the pore structure of the Stanzel rock is unstable in the presence of water. The observed behavior of this sample as well as the above mentioned correlation can be explained as follows: Expandable (non-illitic) clay partly occupies the pore structure of this rock which is mainly a limestone. When saturated, water first fills the rest of the pore space. Then, it

gradually enters the laminar structure of clay where it imitates an ice-like structure (T. Demirel, Ph.D. Thesis, Iowa State University, 1962). Thus clay particles swell and expand towards the pore structure of the limestone skeleton, reducing the volume available for pore water, as well as the pore size. Upon freezing, it is the pore water which freezes, but not the interlaminar water even at the lowest temperature. Since ice-porosimetry measures the pore volume occupied by freezable water, whereas in the conventional gravimetric method the total volume of absorbed water is measured, the difference is the normal volume of interlaminar water. Water molecules in the latter state presumably can not freeze, but do participate in mass transport in pore water \rightarrow ice transition which is responsible for frost damage. In other words, the interlaminar water acts as if it were in a pore of infinitely small size. Thus, the detrimental role of expandable clay in frost damage becomes understandable.

This observation also suggests that porosity determined by ice porosimetry can be a valuable indication for frost susceptibility of clayey rocks when compared with gravimetric porosity. It is an area which appears to be worth studying in the future.

Part 3. Rate of Ice Growth

To assess the possible contributions of various factors which control the rate of growth of bulk ice in contact with a saturated porous medium at a subzero temperature in a non-equilibrium situation, upward movement of a continuously saturated and laterally insulated Vycor rod sitting on a mass of ice was observed at various freezing temperatures. The rate remained constant in spite of the fact that the ice thickness more than doubled during the experiment. This indicated that heat transfer as discussed in the project proposal was not a rate determining factor at a growth rate of about 2 mm/day. For analyzing the contribution of hydraulic permeability of the porous medium

to ice growth rate the vertical temperature profile in the porous medium was established at each temperature. The temperature profile was used to estimate the viscosity (η) of pore water.

Were the rate solely controlled by the hydraulic permeability, it would theoretically be proportional to $-t/\eta$ where t is the temperature at the ice/pore water interface in degrees C and η is the integral mean viscosity of water in the porous column. A plot of the rate against $-t/\eta$ is shown in Fig. 5, which is far from being linear, indicating that another rate determining factor is in operation and that its effect increases as temperature decreases. To investigate the nature of this factor experiments were performed in a cryostat using a 6.6 cm long and 1.45 cm in diameter Vycor (porous glass) rod as shown in Fig. 23. The rate of ice growth at various settings of cryostat temperatures was determined by measuring the upward movement of the porous sample with a cathotometer as the ice grew at the bottom of the sample due to migration of water from the water reservoir on the top of the sample. The temperature profile through the bottom (ice/pore water boundary) to the top of the sample was determined at each of the cryostat temperatures by using a simulated sample equipped with an adjustable thermocouple. The simulated sample consisted of a glass tubing having the same dimensions as the Vycor sample, filled with a fine sand saturated with methyl alcohol. The thermocouple extended through the center to the bottom of the simulated sample for recording the ice/pore water boundary temperature. After the measurement of the boundary temperature the thermocouple was raised through the sample in steps to determine the temperature profile at each cryostat temperature. The temperature profile was used to determine the average density and viscosity of pore water for flow rate calculations. The results obtained are summarized in Table 4. The temperature at the lower end of the porous medium, i.e. at the ice/pore water boundary, is given in the first column of this table for each experiment. These values were

obtained by the simulated temperature measurements. The observed rates are tabulated in the second column.

Table 4.

t Temp. at ice/pore water boundary, °C	q_i Observed rate of ice growth, cm/day	$\bar{\eta}_w$ Mean viscosity of water (a) cp	$-t \eta_w^0 \bar{\rho}_w \rho_w / \bar{\eta}_w \rho_i$ °C g/cm ³
- 1.3	0.050	1.28	1.98
- 5.1	0.154	1.37	7.25
- 6.6	0.195	1.36	9.44
-10.6	0.194	1.50	13.73
-13.4	0.070	1.62	16.03
-13.5	0.060	1.59	16.45
-14.9	0.010	1.67	17.27
-15.7	0.000	1.71	17.78

^aFrom the temperature profile using Handbook values and the Arrhenius equation for extrapolations.

Were the rate of growth of ice controlled only by the hydraulic permeability of the porous medium, the rate could be formulated as follows: If the (gauge) pressure on the ice phase p_i is zero, Eq. (1) of the project proposal, i.e.

$$p_i = \rho_i p_w / \rho_w + \rho_i \lambda (-t) / T_0 \quad (1)$$

where p_w is the pore water (gauge) pressure and t is the temperature in °C at the ice/pore water boundary, i.e. at the lower end of the Vycor rod, T_0 is the normal melting point of ice in °K, λ is the heat of fusion of ice per unit of mass, ρ_i and ρ_w are the density of ice and water, respectively, at temperature t ; leads to

$$p_w = \lambda \rho_w t / T_0 \quad (1a)$$

Numerically Eq. (1a) can be written as

$$p_w = 12.0 \rho_w t \quad (1b)$$

which expresses p_w in atmospheres, using ρ_w in g/cm^3 . It must be noted that the pore pressure p_w at the lower end of the porous medium at subfreezing temperatures is negative. For instance, for $t = -1^\circ\text{C}$ $p_w = -12$ atm. (gauge). At the upper end, the pore pressure is atmospheric. Then, the pressure gradient across the whole length of the Vycor rod is equal to $12.0 \rho_w(-t)$. The linear rate of flow of pore water q_w can be expressed by applying Darcy's law as

$$q_w = 12.0 \rho_w (-t) K/L \quad (2)$$

where K is the hydraulic permeability and L is the length of the porous medium. Because of the temperature gradient in the vertical axis, K is the mean hydraulic permeability. If K_0 is the hydraulic permeability measured at 0°C , K is calculable by

$$K = K_0 \eta_w^\circ / \bar{\eta}_w \quad (3)$$

where η_w° is the viscosity of water at 0°C and $\bar{\eta}_w$ is the integral mean of this viscosity. The latter was calculated by graphical integration of

$$\bar{\eta}_w = (1/L) \int_0^L \eta_w dL \quad (4)$$

Values of η_w were obtained from handbooks and the Arrhenius equation for extrapolations using the temperature profile obtained by simulated temperature scanning along the vertical axis. The values obtained are tabulated in the third column of Table 4 at each observation point.

On the other hand, the linear rate of growth of ice q_i is correlated to the rate of water flow by

$$q_i = q_w \bar{\rho}_w / \rho_i \quad (5)$$

where $\bar{\rho}_w$ is the mean density of pore water which was also computed from handbook data. From Eqs. (2), (3) and (5) we obtain

$$q_i = 12.0 K_0 \eta_w \rho_w \bar{\rho}_w (-t)/L \bar{\eta}_w \rho_i \quad (6)$$

To obtain q_i in cm/day, L is measured in cm and K_0 is expressed in $\text{cm}^2/\text{atm. day}$.

Equation (6) implies that if the growth rate is controlled only by hydraulic permeability, a plot of this rate versus $-t \eta_w^\circ \rho_w \bar{\rho}_w / \bar{\eta}_w \rho_i$ should be linear with a slope of $12.0 K_0/L$. The values of the former quantity are tabulated in the fourth column of Table 4. The rate of ice growth is plotted against this quantity in Fig. 6.

Although the plot appears to be linear in the vicinity of 0°C , as the temperature is lowered, the rate increases less and less than expected, and eventually passes through a maximum at about -9°C , then decreases drastically and becomes zero at -15.7°C .

To draw the straight line expected from Eq. (6), hydraulic permeability, K_0 , of Vycor was measured at 0°C using a 0.566 cm thick and 1.45 cm in diameter disc in the usual manner. K_0 was found to be $0.0171 \text{ cm}^2/\text{atm. day}$. The straight line obtained with this value is shown in Fig. 6. The perfect agreement between this line and the experimental curve at temperatures close to 0°C is an evidence not only for the fact that the rate is determined only by the hydraulic permeability within this temperature range, but also for the validity of the pressure relationship (i.e. Eq. (1), also in the Project Proposal) and the underlying theory.

The observed deviation from the straight line at lower temperatures in the manner described above cannot be attributed to capillary freezing, since both conductometric and dilatometric studies show that capillary freezing in Vycor starts at -17°C even under equilibrium conditions. Nor can it be attributed to

a retardation caused by conduction of heat through the bulk ice on the basis of constant rate of ice growth. Whatever causes this trend is other than heat transfer.

It appears that the retardation is strongly correlated to temperature: The lower the temperature, the larger is the retardation. This suggests that the third rate determining factor as considered in the Project Proposal is in operation: It is the viscous flow of ice. Although the experimental system did not involve any massive flow of ice, the growth of ice at the ice/pore water boundary depends on transport of ice at the microscopic level from the ice built up on the ice menisci at the openings of micropores to the exterior. What causes this transport is apparently a pressure gradient developed continuously at each ice/water meniscus. When the dynamic steady state is attained, the ice pressure at the meniscus must be somewhat higher than atmospheric. In other words, p_i is no longer zero, and the total pressure gradient across the porous medium is not $12 \rho_w(-t)$ but is $12 \rho_w(-t) - p_i \rho_w/\rho_i$ as required by Eq. (1). This, in turn, lowers the rate.

The absence of this effect in the vicinity of 0°C indicates that the viscosity of ice at 0°C is not large enough to manifest itself. At lower temperatures, however, ice apparently becomes more and more viscous causing retardation in phase transition.

In conclusion it can be stated that in the vicinity of freezing point hydraulic flow through capillary pores gives rise to rapid formation of ice lenses whereas at very low temperatures, but above capillary freezing point, viscous flow of ice becomes the controlling factor and the growth rate drops sharply due to increasing viscosity of ice. This observation also explains the well known phenomenon of extreme frost susceptibility of porous materials at mild freezing temperatures generally blamed on only freezing-thawing cycles. It should also play an important role in design of insulations and durability tests.

Part 4. Overview of Frost Action on Rocks and Concretes

The fundamental studies carried out within this project revealed the validity of the theory of plastic ice in freezing and thawing in capillary media. The theory implies that ice in the capillaries behaves as a plastic mass rather than a crystalline solid, exhibiting a convex meniscus against water in the capillary with zero contact angle. Capillary freezing and melting is nothing but virtual movement of the ice/water boundary in one direction or the other. The model does not rule out the mechanism of "in-situ" nucleation in freezing, but can predict what happens when ice is once formed somewhere in the system. If the bulk water surrounding a saturated porous sample freezes first, then the theory can predict any behavior of the system such as freezing and melting points in a capillary of given size and geometry, also the pressure in one phase relative to that in the other phase. Therefore, the model is indispensable for prediction of frost action in porous materials of geotechnical and engineering importance.

The underlying thermodynamics can be summarized by a few simple numerical equations. Namely, if p_i and p_w are the ice and water (e.g. gauge) pressures in atmosphere, respectively, and r is the radius of curvature of ice/water interface in μm , then

$$p_i - p_w = \frac{0.59}{r} \quad (7)$$

which follows from the Laplace equation. When $p_i = 0$ (i.e. ice is under atmospheric pressure)

$$p_w = 12 \, t \quad (8)$$

and

$$t = -0.049 / r \quad (9)$$

where t is the temperature in $^{\circ}\text{C}$. When $p_w = 0$ (i.e. water is under atmospheric pressure),

$$p_1 = -11 t \quad (8')$$

and

$$t = -0.053 / r \quad (9')$$

Let us discuss within this theory what happens to a water filled spherical pore of say $5 \mu\text{m}$ radius in a rigid material, such as concrete, connected to the surface covered with ice by a cylindrical capillary channel of say $0.005 \mu\text{m}$ in radius (Fig. 24a). Such a cavity appears to be the source of frost damage. Equation (9) predicts that the cavity will freeze at about -10°C determined by the radius of the channel by virtual penetration of the surface ice, while Eq. (8) tells us that until that happens the pressure inside the cavity decreases as much as to -120 atm . During freezing, since some ice must be pushed out of the capillary channel due to expansion on freezing, a large pressure gradient becomes operative along this channel. On thawing, the reverse will take place. However, the melting point will be much higher, because it is determined by the radius of the cavity itself. Ice in the cavity melts, according to Eq. (9) practically at 0°C (to be exact at -0.01°C).

The structure will probably survive after this temporary stress it suffers during freezing and thawing. In practice, however, such cavities are usually also connected to the groundwater by other capillaries (Fig. 24b). In this case at -10°C the cavity will suck groundwater continuously. This will partially release the negative pressure in the cavity. Under these conditions, as Eq. (7) indicates, the pressure requirement for freezing the upper capillary channel is

never fulfilled. Therefore, the system will remain unfrozen. Now, the system is in a non-equilibrium state, and there will be a continuous pore water \rightarrow bulk ice phase transition at the top.

If temperature drops further, the fate of the system depends on the occurrence of one of the two following processes:

(a) The hydraulic head loss due to liquid flow may lower p_w , on one hand, and the lag in viscous adaptation of ice meniscus may increase p_i at the ice/water interface. The experimental results presented in Progress Report 4, Part II and also presented in Figure 6 indicate that both of these phenomena are in operation almost to the same extent at around -10°C . These changes in pressures may restore the freezing condition required by Eq. (7) and result in freezing of the system.

(b) The cavity may freeze by "in-situ" nucleation.

Freezing experiments made with cement paste in contact with bulk ice seem to indicate that freezing under non-equilibrium conditions takes place by mechanism (a) rather than mechanism (b).

One point is certain that the cavity under consideration will not freeze at -10°C and its partially released negative pressure (e.g. at -50 atm.) will be maintained.

At temperatures somewhat below -10°C this cavity should freeze and cause the freezing zone to penetrate deeper as far as to a depth whose temperature is -10.6°C according to Eq. (9'), provided that the same pore structure repeats itself in the vertical direction. Now let us consider a similar cavity at the boundary of the freezing zone, which is frozen and connected to the groundwater by an unfrozen capillary channel (Fig. 24c). Because of extremely high viscosity of ice at these temperatures, the rate of upward flow of ice will be practically null. Therefore p_i in this cavity will practically assume its equilibrium value given by Eq. (8') which was verified experimentally as

described in Part I of this report. According to this equation the equilibrium gauge pressure at -10.6°C is $p_i = 117 \text{ atm.}$ which is a potential source of frost damage.

If the surface temperature and, therefore, the temperature at this cavity increases, the ice pressure decreases in accordance with the Eq. (8'). In other words, this equation describes the variation of p_i in the temperature interval of $-10.6^{\circ}\text{C} < t < -0.01^{\circ}\text{C}$ (melting point of ice in the cavity).

However if the surface temperature drops, the ice/water boundary travels deeper to a depth where $t = -10.6^{\circ}\text{C}$, provided that there is a vertical temperature gradient. Therefore the ice pressure at the boundary will be 117 atm.(gauge) again, and become independent of the surface temperature, as discussed in the Project Proposal. What controls this maximum ice pressure is the size of the capillary channels, more correctly, the pore constrictions. Indeed, we can obtain the correlation between the maximum ice pressure and constriction radius from Eq. (7) by setting $p_w = 0$ as

$$(p_i)_{\max} = \frac{0.59}{r} \quad (7')$$

This ice pressure is exerted in the structure when the surface temperature t is given by (see Eq. (9'))

$$t \leq -0.053 / r \quad (9'')$$

The chart in Fig. 25 shows the dependence of ice pressure on temperature according to Eq. (8') and the maximum pressure attained with pore constrictions of various radii according to Eq. (7').

Equation (7') predicts that the smaller the constriction size, the more frost susceptible is the material.

Mercury intrusion studies by W. Dubberke on dolomite and limestones of known durability and field service appear to support this general expectation,

It follows from Eq. (7) that development of a negative absolute pore pressure is a prerequisite for freezing a water filled cavity connected to the surface by a channel smaller than $0.59 \mu\text{m}$ in radius. If some of the interconnected cavities are initially filled with air, since pore water \rightarrow bulk ice transition which is the precursor of capillary freezing, does not effect the gas content of the system, the state of negative pore pressure can never be attained in the presence of a gas in the system, unless it is confined in a volume behind a very narrow connecting capillary or a neck. Otherwise, in the early stage of pore water \rightarrow bulk ice transition, air should get segregated partly and sandwiched between pore water and bulk ice, sealing pore water from the bulk ice, thus stopping the detrimental phase transition. As an example, a quantitative follow-up based on combined application of the Laplace equation and the Boyle Law, of the consequence of connecting an air pocket of the same size to the water filled cavity in Fig. 24 (b) is presented in Figs. 26 a,b, and c. If the connecting channel is wider than $0.03 \mu\text{m}$ in radius (Fig. 26a) air will push the cavity water out to freeze outside and release the negative pore pressure (Fig. 26b). Since the mass transfer stops at this stage, pore water resumes its normal value. Then it fills in both cavities partly (Fig. 26c). Thus a static equilibrium is reached. If the channel connecting the two cavities is narrower than $0.03 \mu\text{m}$ in radius, air would have no effect.

Wide enough connections between the cavities to allow this process to occur should and may be present in air entrained concrete, formed by air bubbles sticking to water filled cavities in the cement phase or to the aggregate surface before setting (Fig. 26d). Such a wide connection may also be created between an unconnected air pocket and a close-by water-filled cavity by the collapse of the partition between them owing to high negative pressure in the latter under frost conditions (Fig. 26e).

Preliminary experiments made on air entrained cement paste in a saturated state in the early stage of the project, using the method of electrical conductance, have shown that in the absence of bulk ice a partial capillary freezing takes place at -11°C , evidently by "in situ" nucleation. It is interesting to note that -11°C is also the (supercooled) freezing point of bulk water equilibrated with cement paste. This means that the sample contained some large cavities filled with water which behave as bulk water. Therefore, partially filled cavities of large size as illustrated in Fig. 26 (c) are also expected to freeze by "in situ" nucleation under severe frost conditions. Also in the case of partially filled cavities, the freezing process is confined to the interior of the mass, rather than extending to the exterior, and thus causing no apparent volume increase. Our most recent - but limited - dilatometric freezing experiments made with a 7% air entrained mortar sample, without resorting to an exhaustive presaturation as in porosimetric experiments, appear to confirm this model. Because of the cushioning effect of the trapped air in them, the partially water-filled cavities may not experience high expansive pressures upon freezing, at least for a long time. This may be the mechanism of protection of concrete from frost damage by entrained air.

Since our studies within the present project were mainly confined to the behavior of the three-phase system matrix/water/ice, we do not have conclusive experimental evidence to verify these expectations concerning the presence of air pockets as a fourth phase in the system. Similar fundamental studies on the four-phase system of matrix/air/water/ice appear to be a very interesting research area to be explored in the future in view of its bearing on actual conditions in the field.

Conclusions

1. Ice (phase transition) porosimetry has been fully developed and found superior to mercury porosimetry, since it is capable of measuring both neck and body size of pores, whereas mercury porosimetry measures only neck size as the effective pore size and thus overestimates pore volume associated with that size.

2. Detailed information on pore structure, such as body-size as well as neck-size, is needed for prediction of expansive pressures and frost susceptibility.

(a) Occasional presence of globular macropores interconnected by micropores or constrictions appears to be the source of frost damage.

(b) In general, the smaller the constrictions or micropores the poorer is the performance.

(c) Under severe frost conditions, however, the difference between performance of smaller or larger micropore materials becomes less important, due to extremely slow growth of ice at extremely low temperatures.

3. Also because of small rate of ice growth at low temperatures, upper concrete structures are more resistant to damage under severe frost conditions than under mild conditions.

4. Non-illitic clays in aggregates may behave as micropores of infinitely small size and contribute to poor performance. Ice porosimetry may be used to detect this contribution.

5. Freezing conditions in the field are expected to distribute entrained air in concrete to water-filled cavities. Air in these cavities is, in turn, expected to

- (a) Hinder freezing under mild frost conditions,
- (b) Confine freezing process to occur under severe frost conditions within the interior of the mass, by in situ nucleation, rather than extending to the exterior, and
- (c) Acting as a damper in the cavity, reduce heaving pressure.

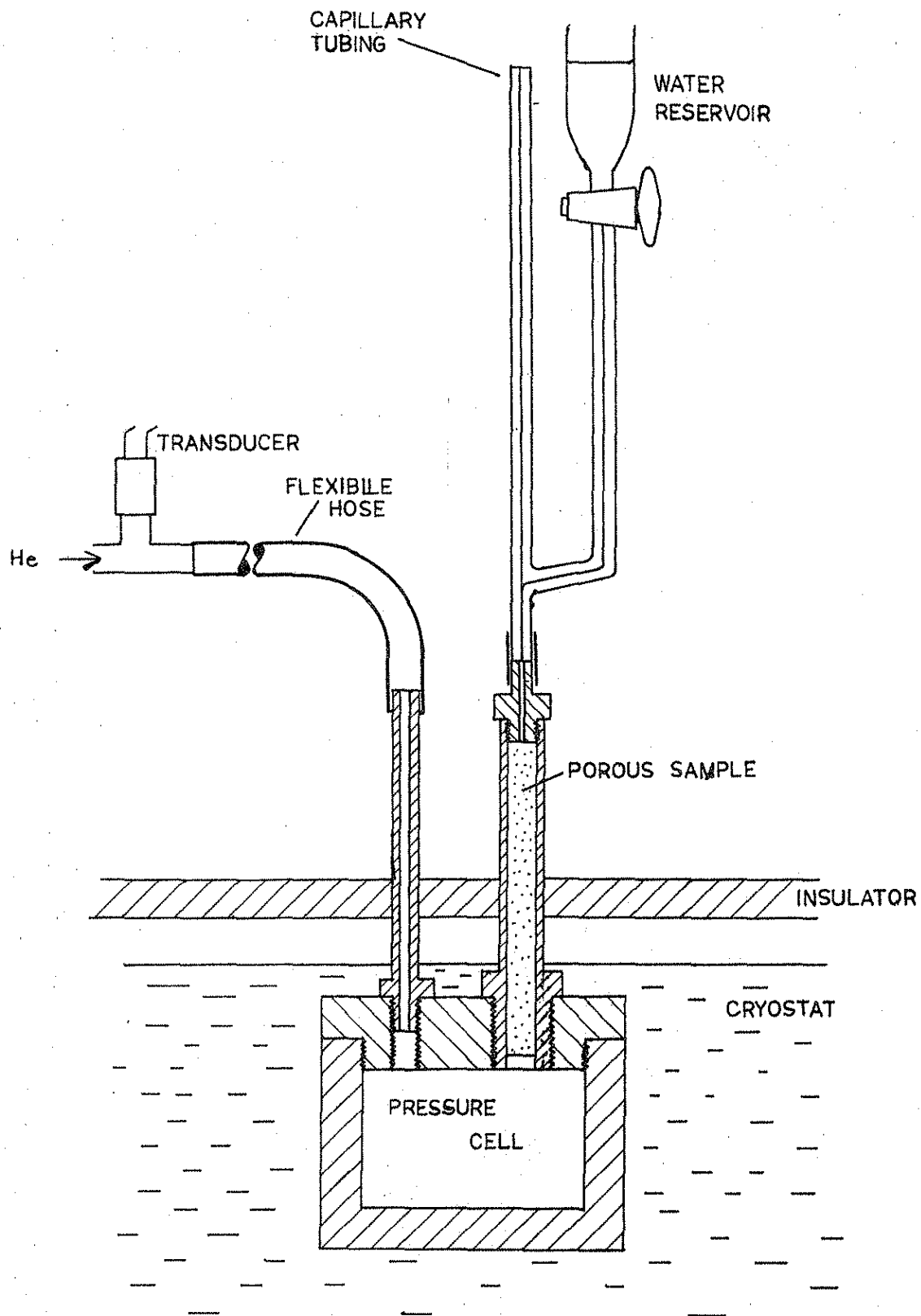


Fig. 1. Apparatus for ice pressure measurements.

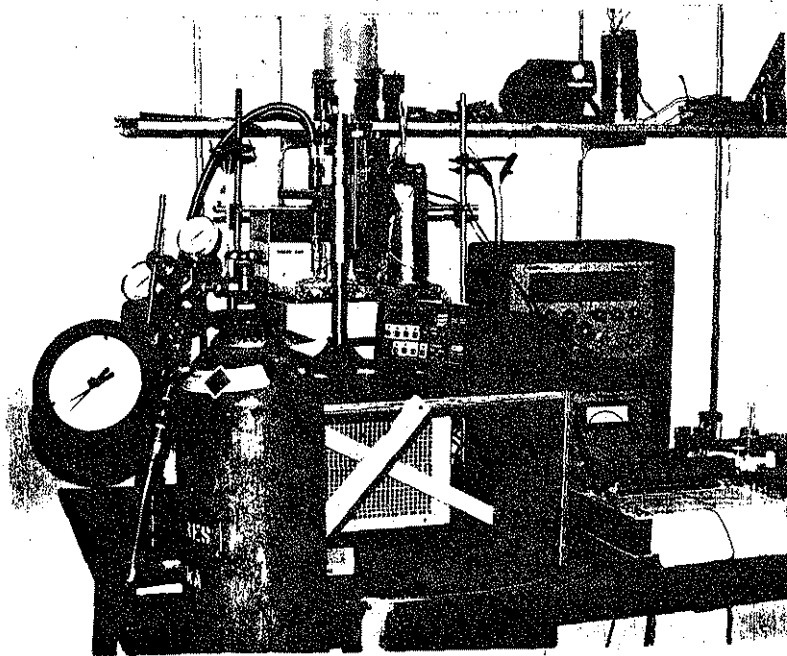


Figure 2. Apparatus for ice pressure measurements.

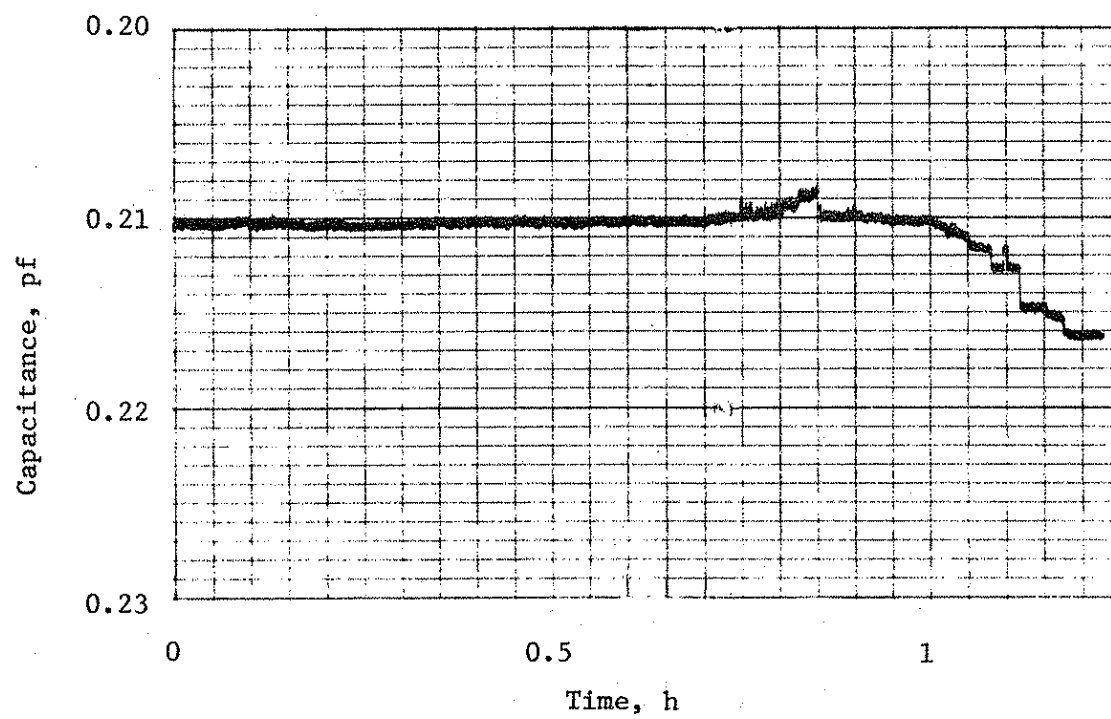


Figure 3. Flow-meter recording at -4.03°C and 700 PSIA.

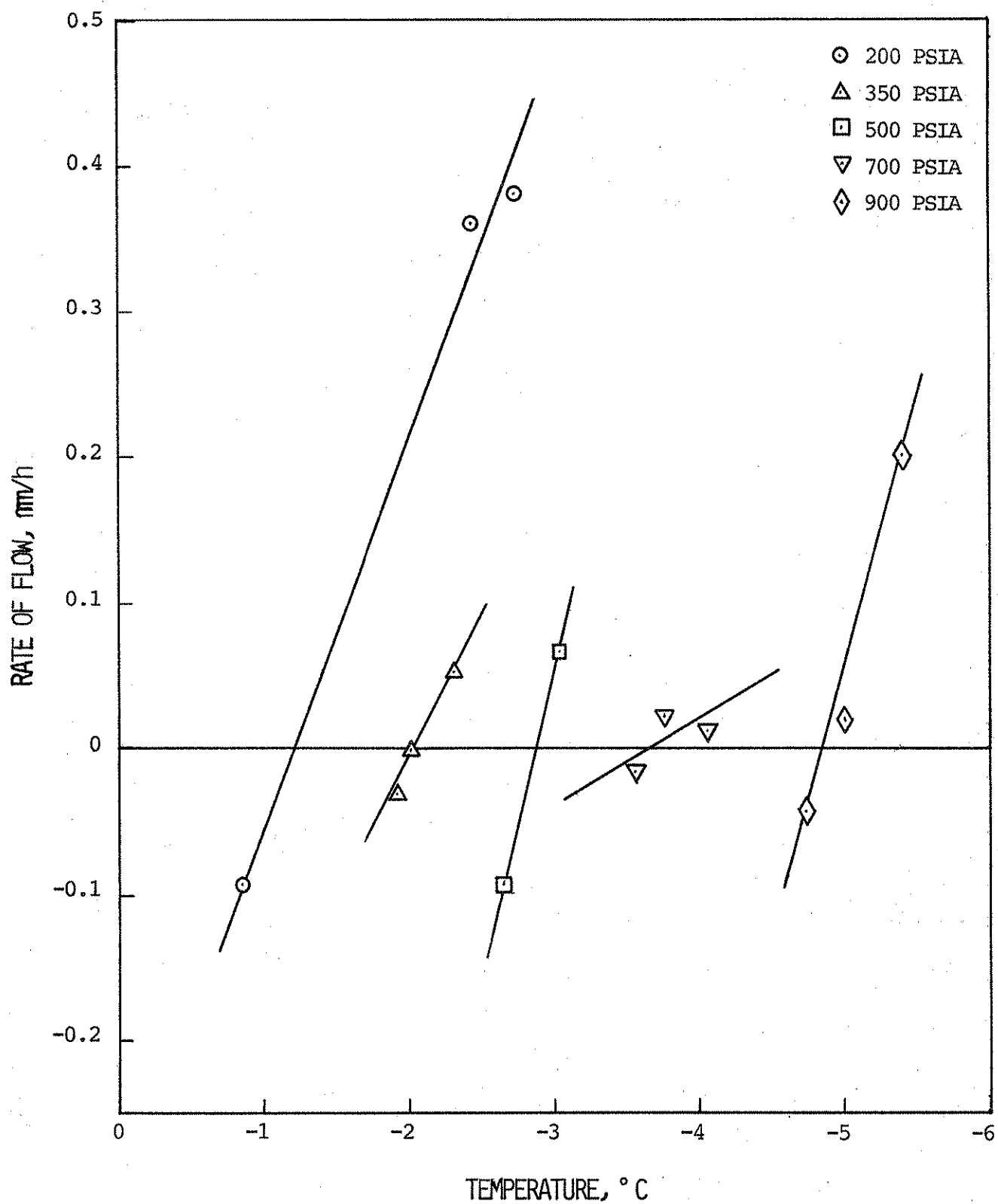


Figure 4. Measured rate of flow versus temperature at various pressures.

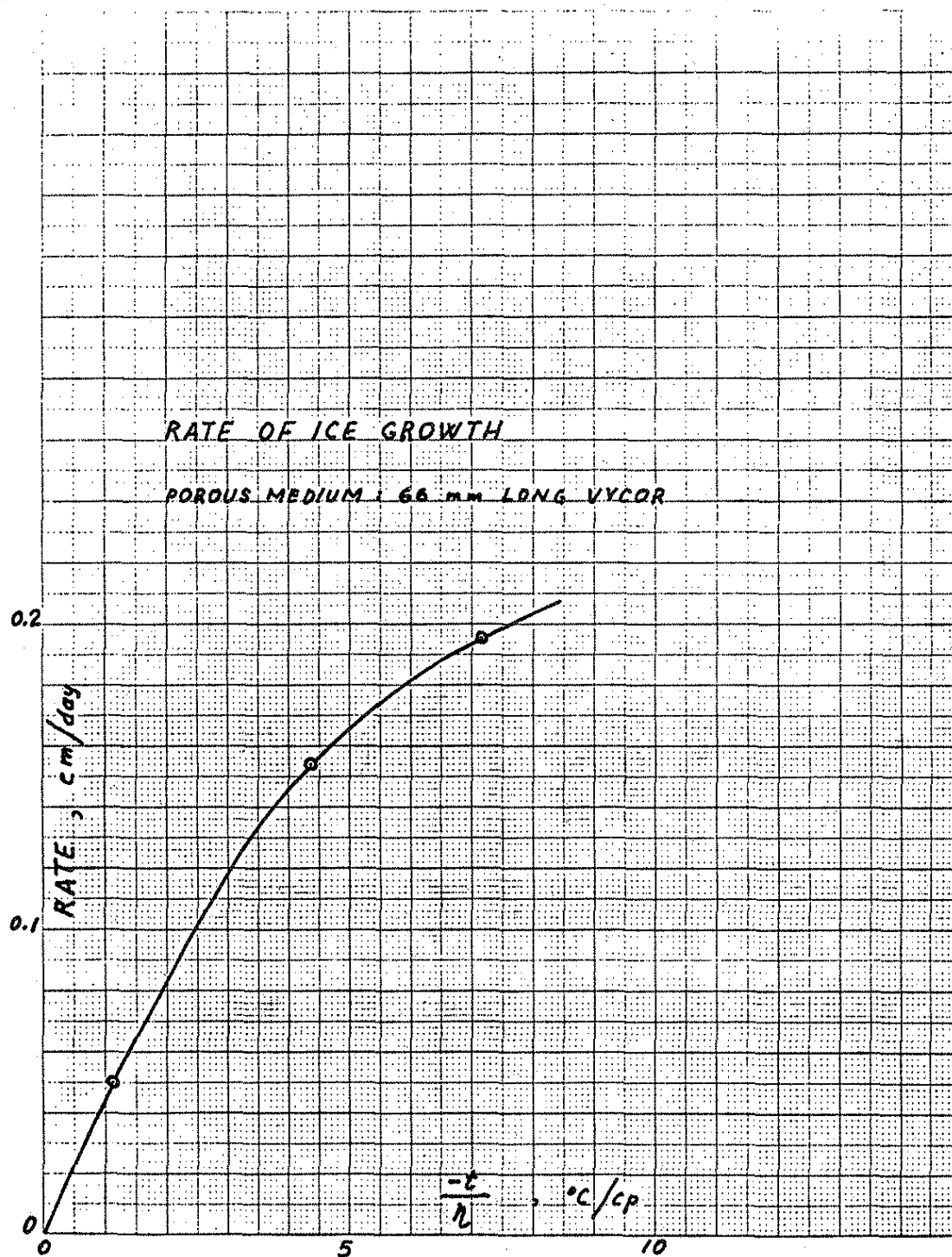


Figure 5. Rate of vertical growth of ice through migration freezing plotted versus $-t/\eta$.

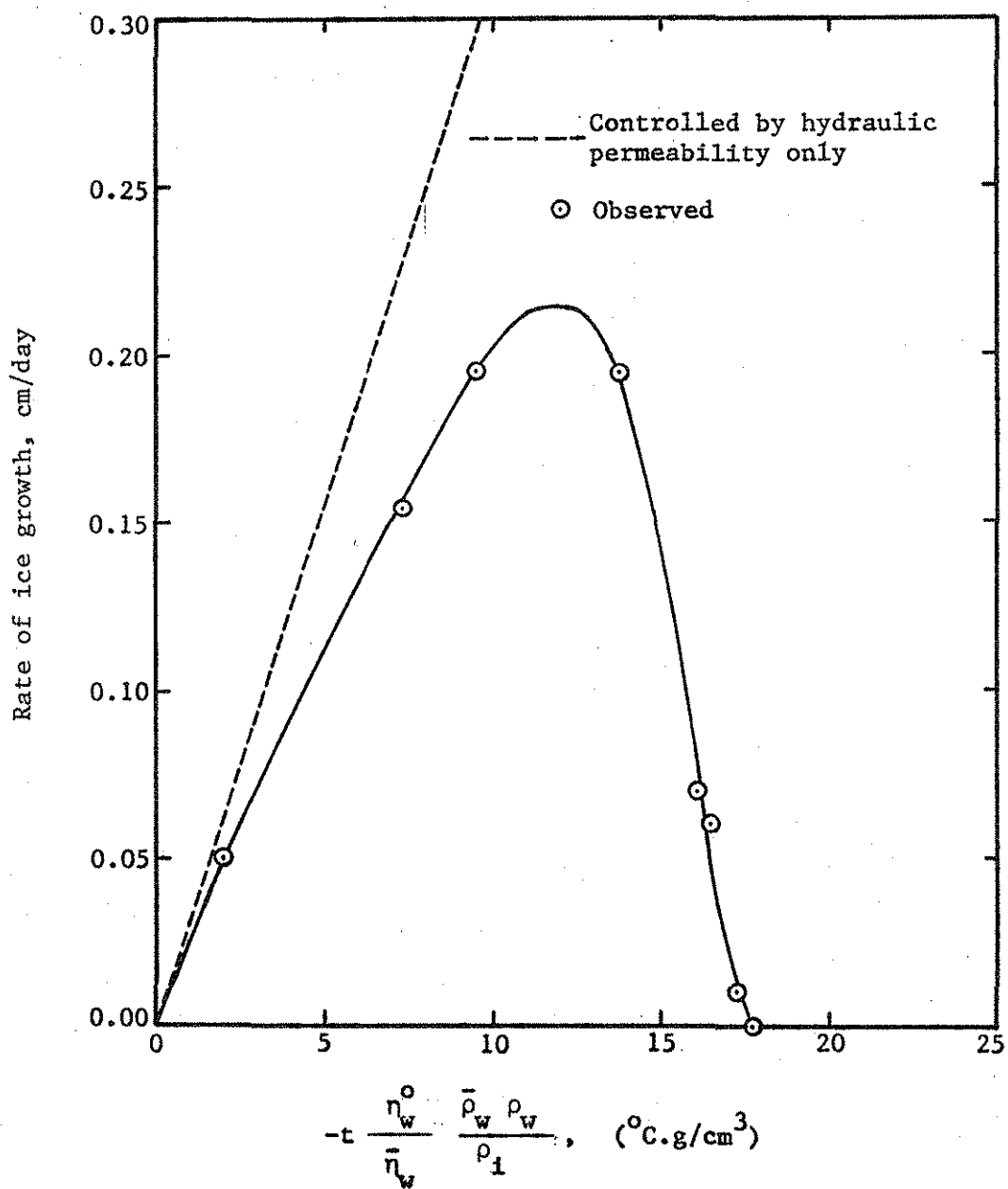


Figure 6. Rate of ice growth as a function of the freezing front temperature.

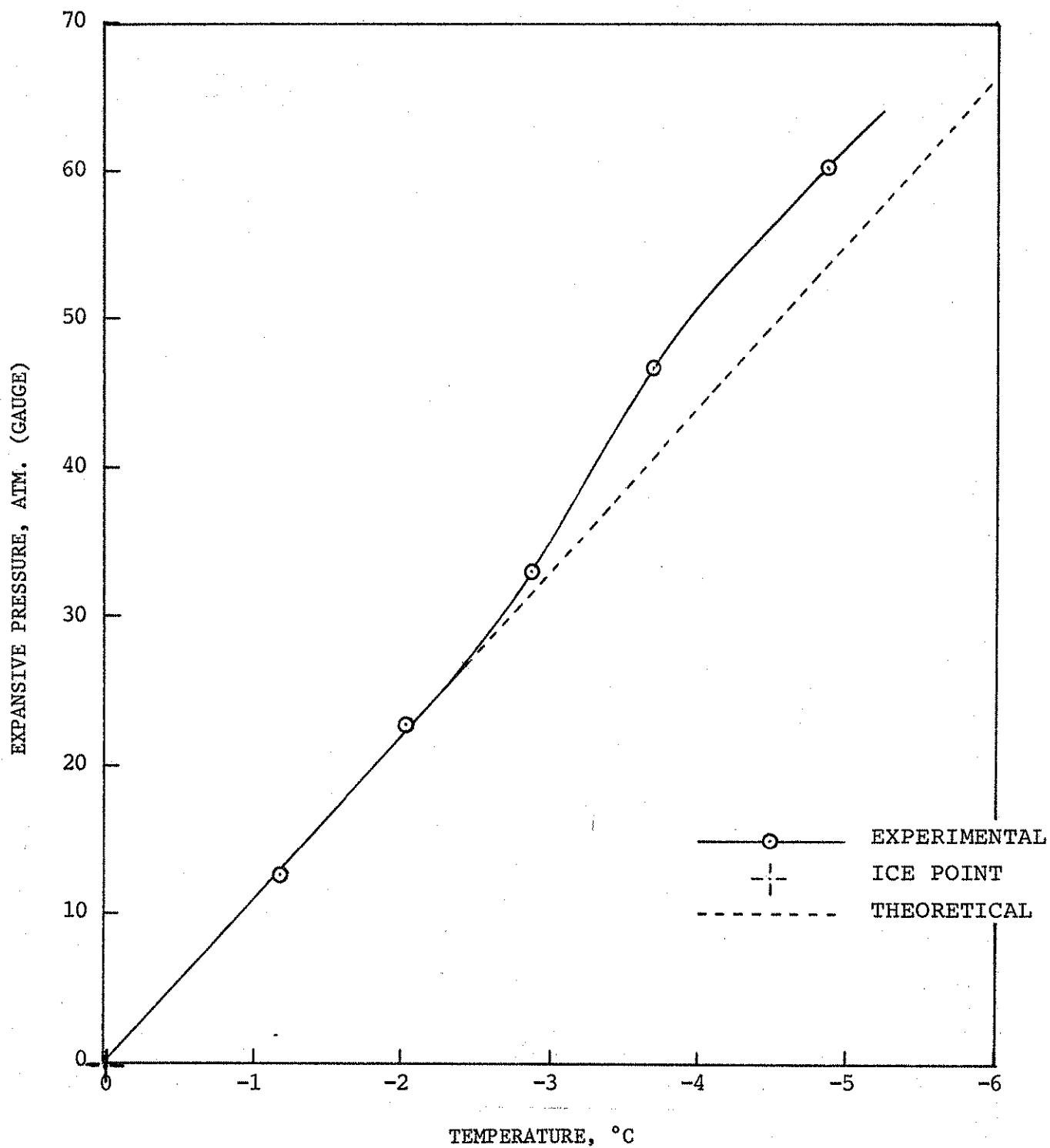


Figure 7. Expansive pressure versus temperature.

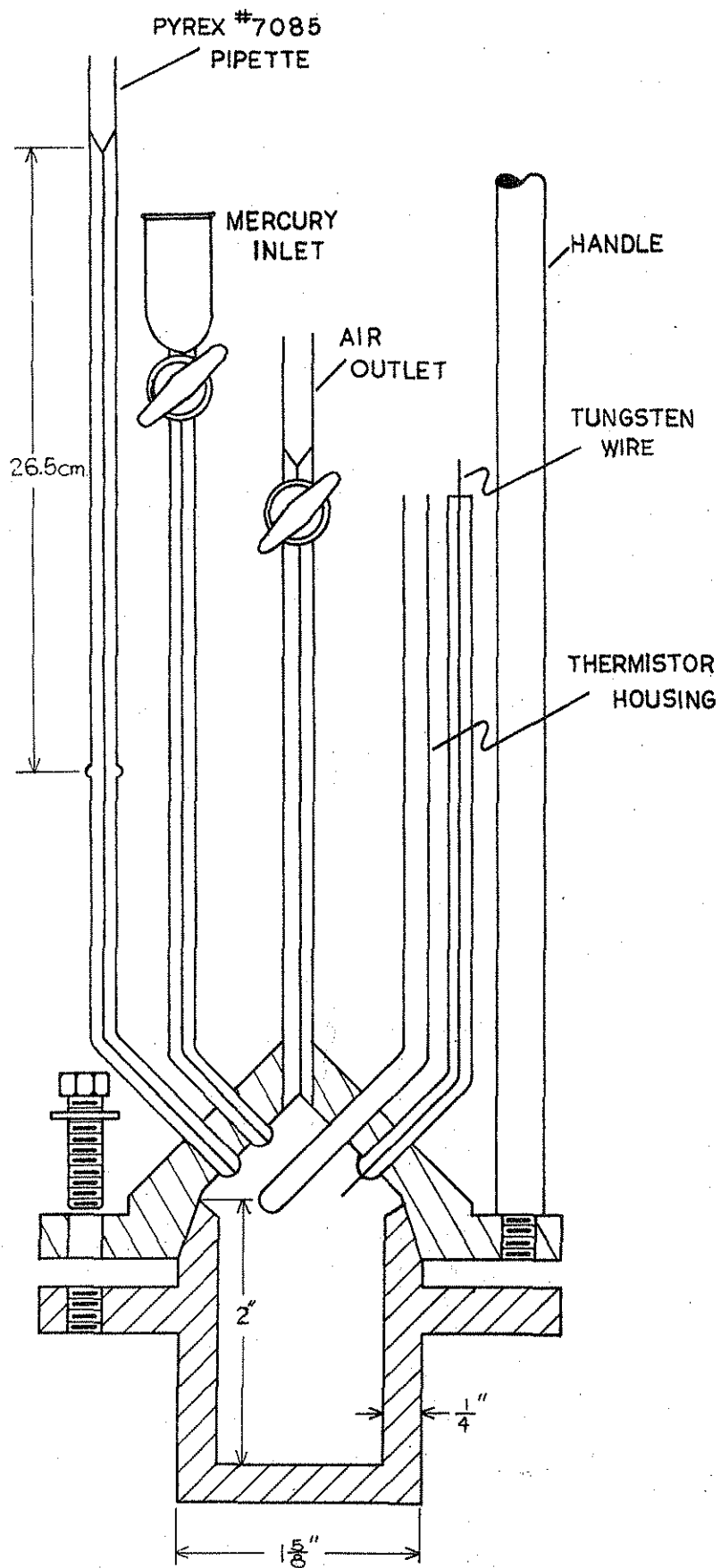
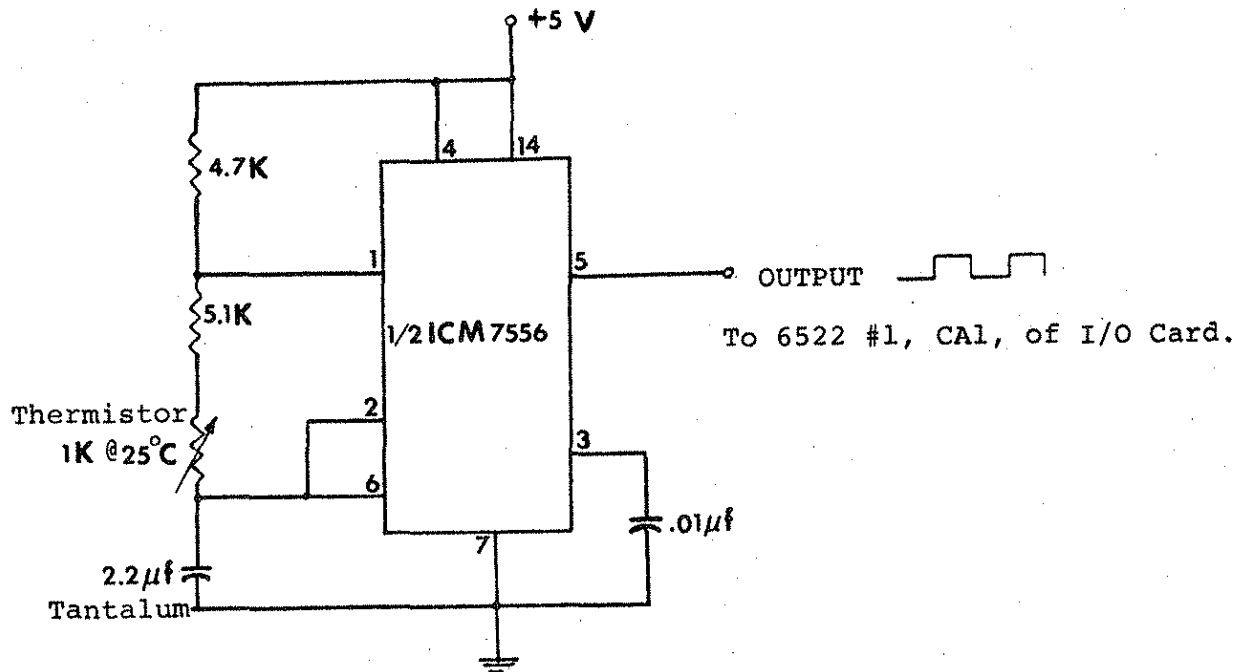
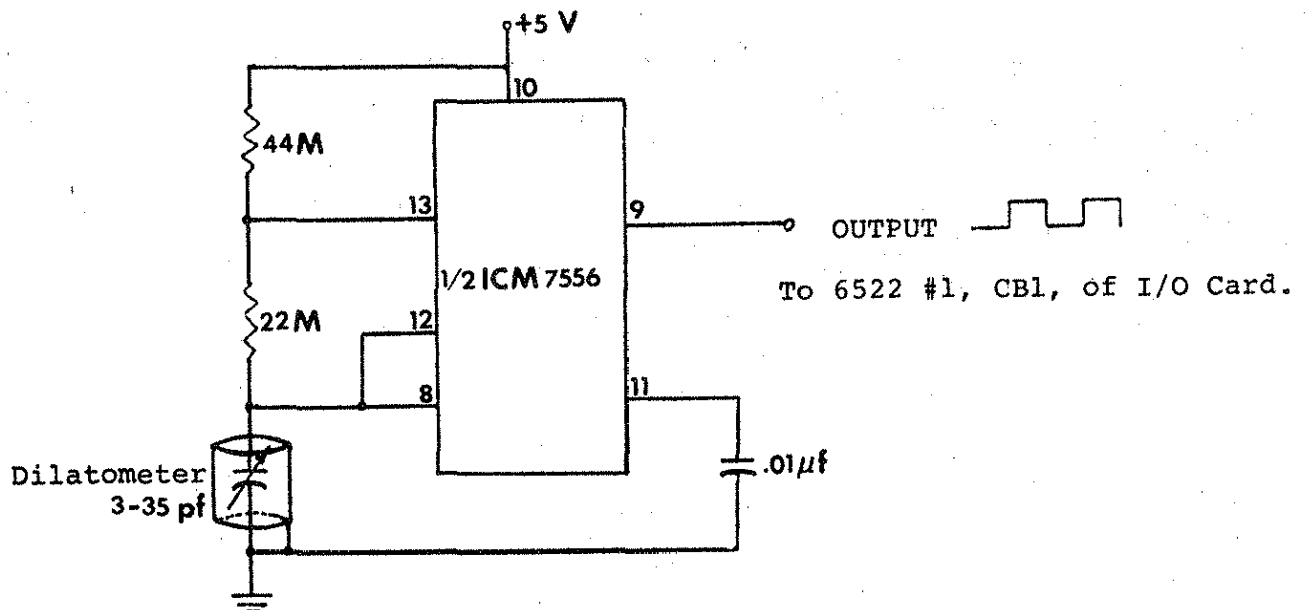


Figure 8. Lexan Dilatometer.



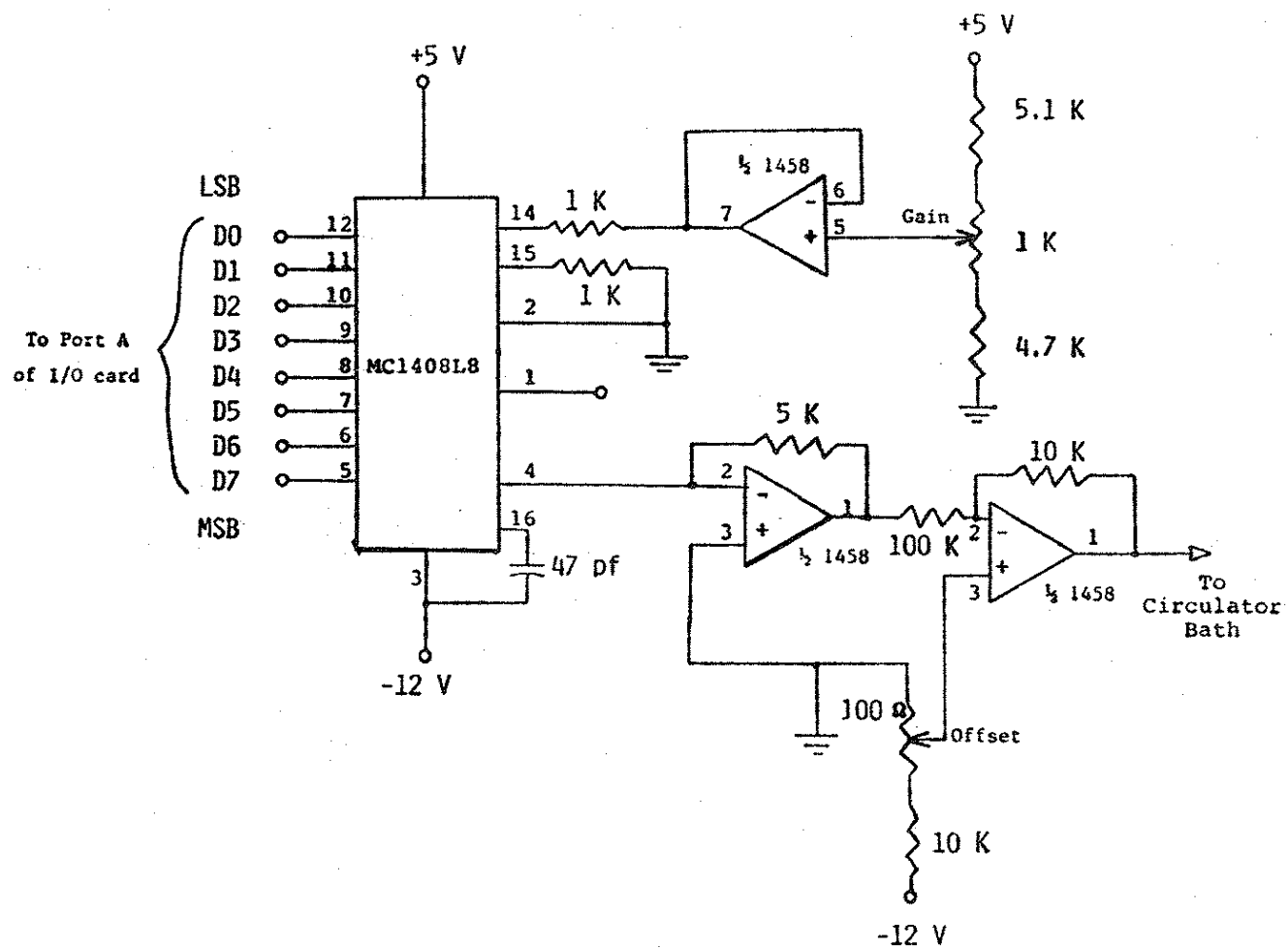
Temperature Circuit



Volume Circuit

Figure 9. Oscillator Circuitry.

Figure 10. Digital to analog convertor.



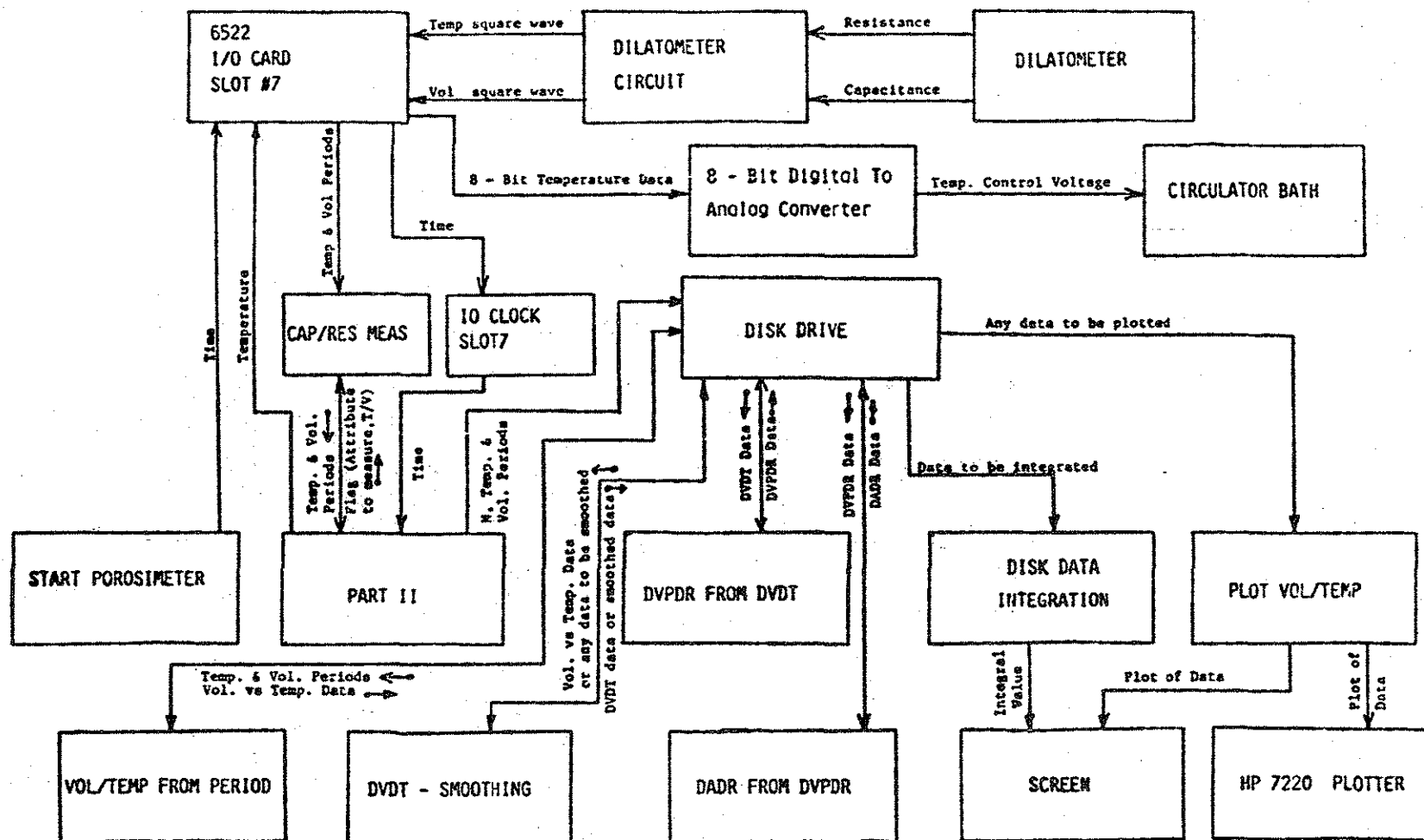


Figure 11. Porosimeter Flow Diagram.

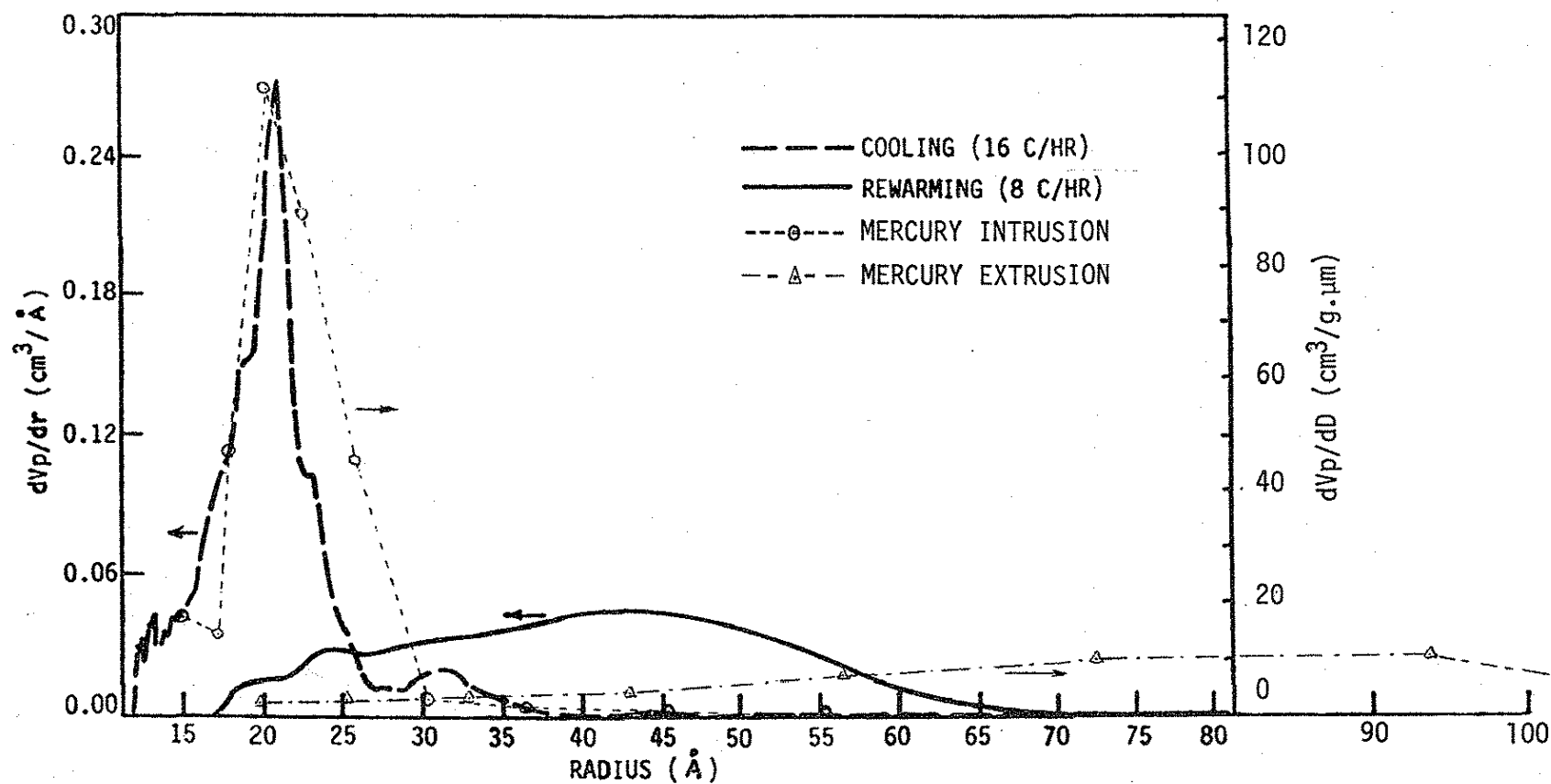


Figure 12. Pore body size (—) and pore neck size (----) distribution of Vycor (5.55 cm³) by phase transition porosimetry, and by mercury porosimetry.

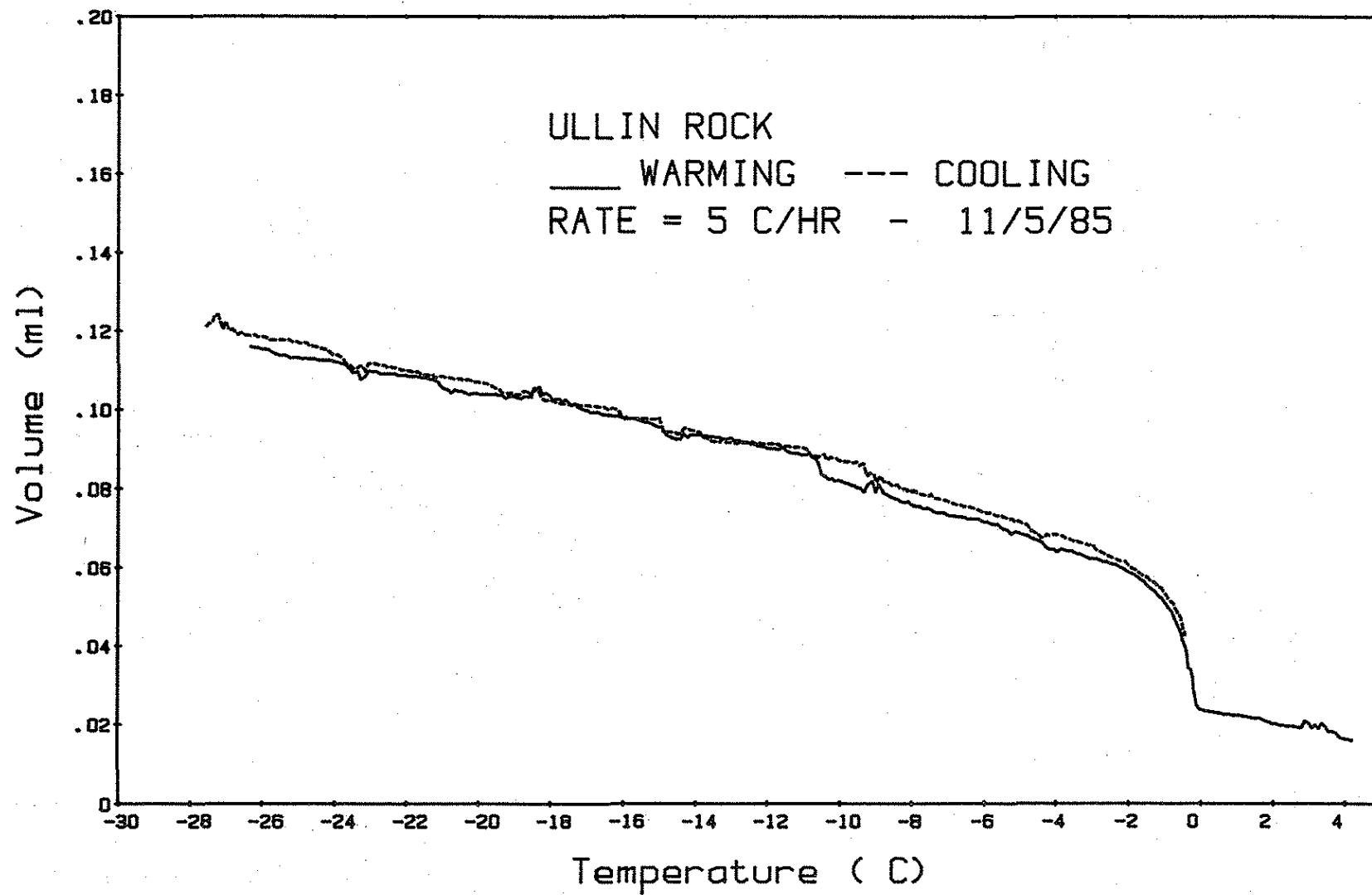


Figure 13. Ice porosimetry of Ullin.

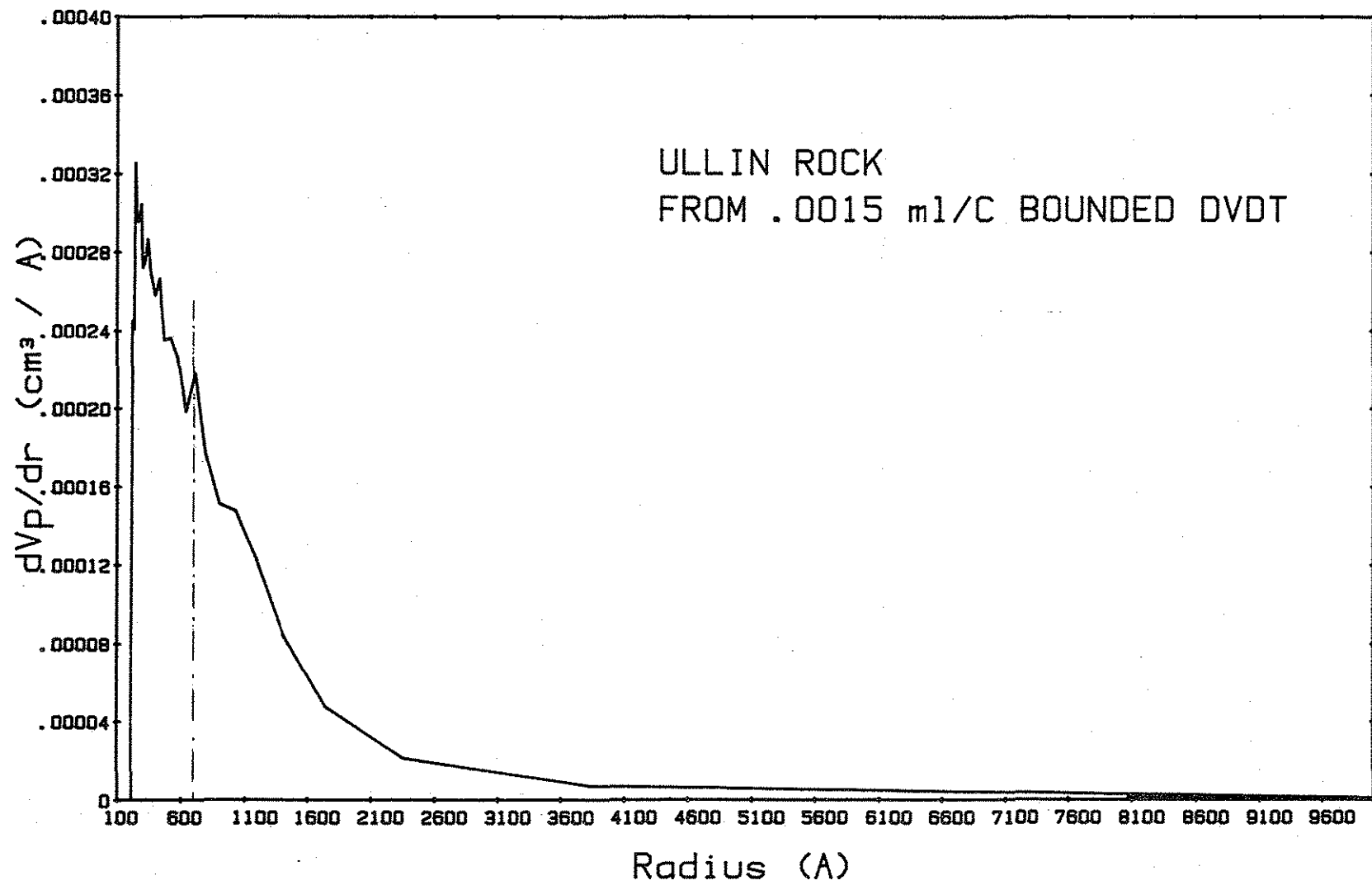


Figure 14. Pore (body) size distribution of Ullin by ice porosimetry,
(mercury intrusion median pore size by W. Dubberke).

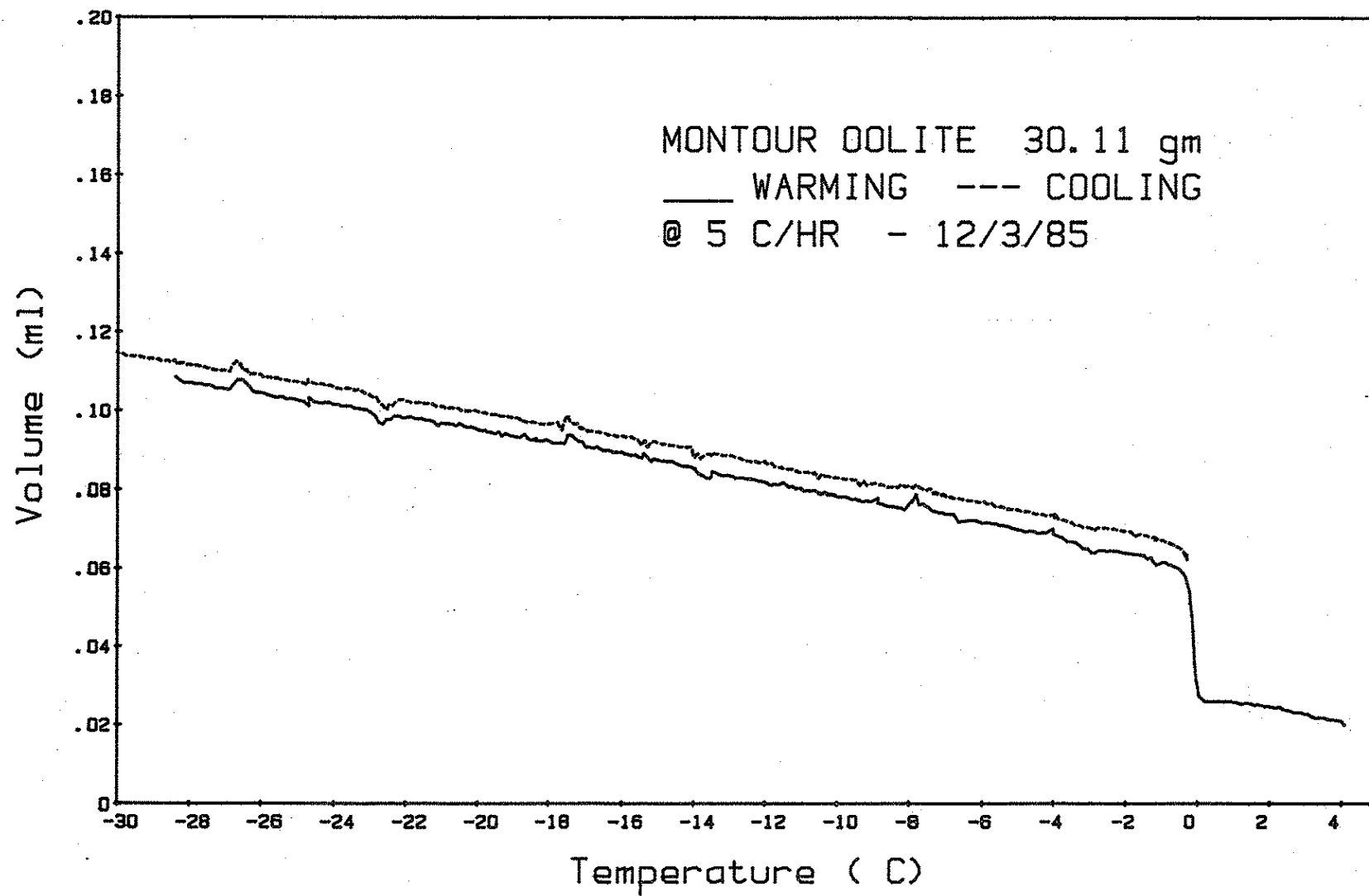


Figure 15. Ice porosimetry Montour Oolite.

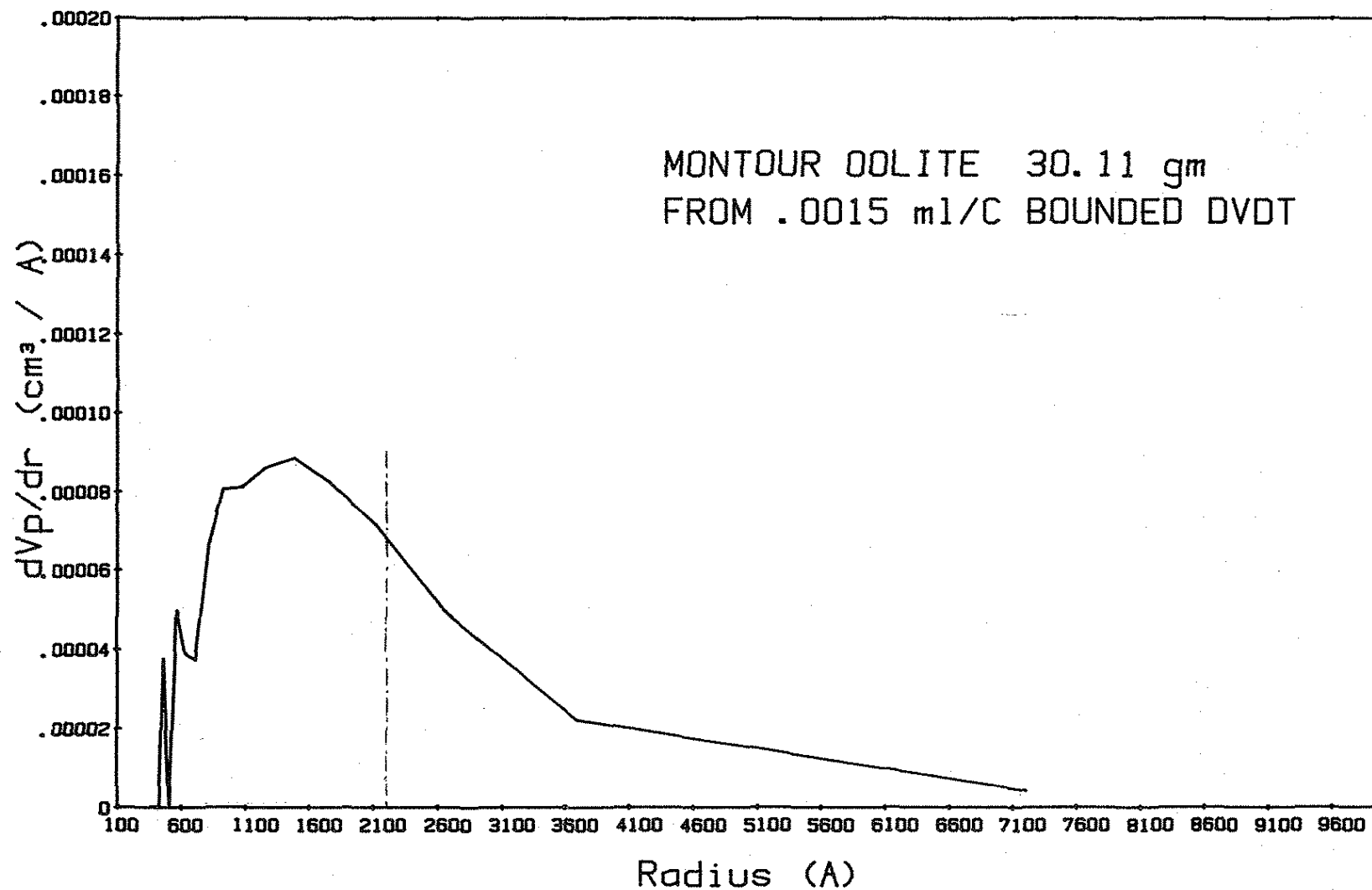


Figure 16. Pore (body) size distribution of Montour Oolite by ice porosimetry,
(mercury intrusion median pore size by W. Dubberke).

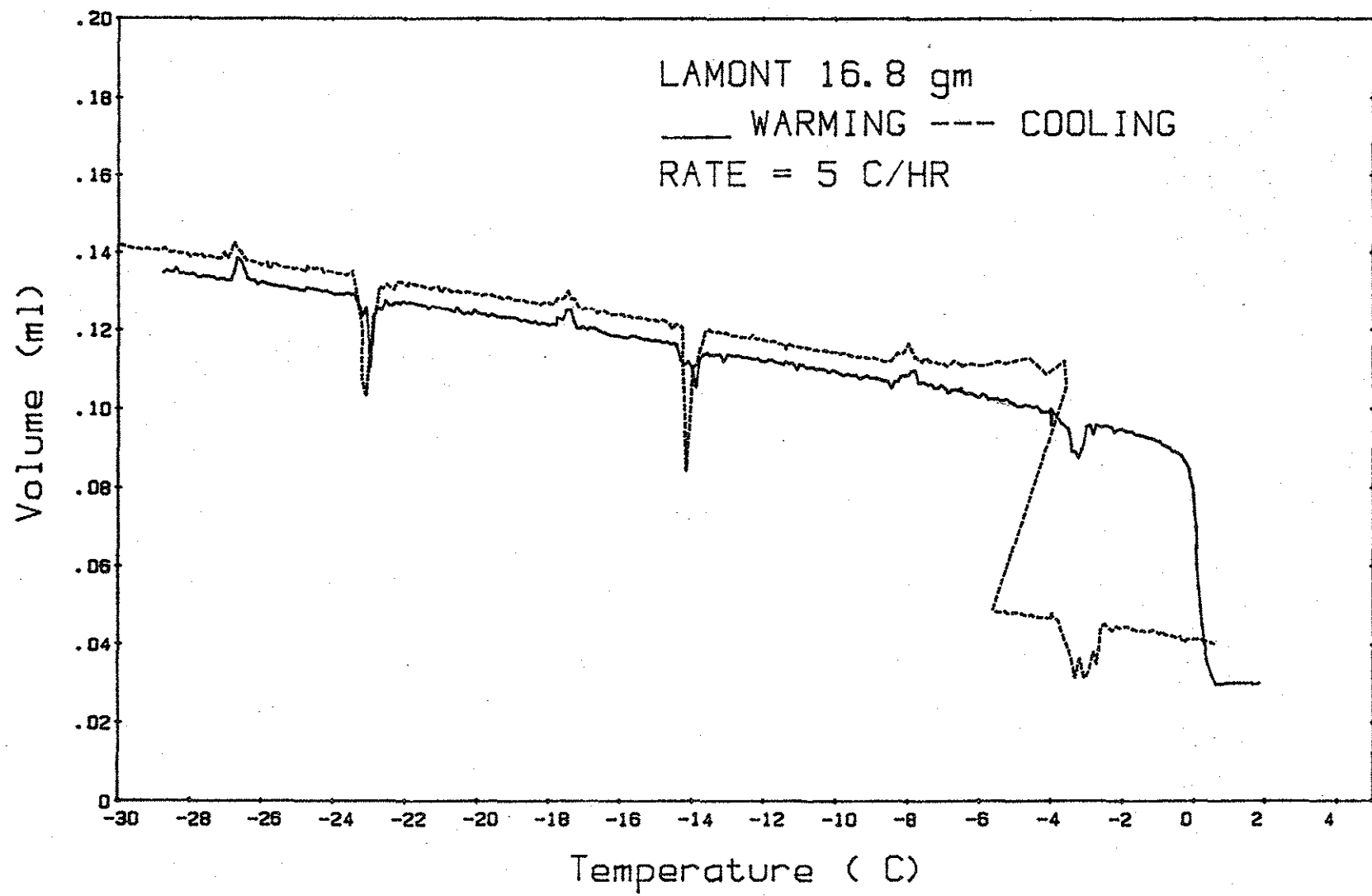


Figure 17. Ice porosimetry of Lamont.

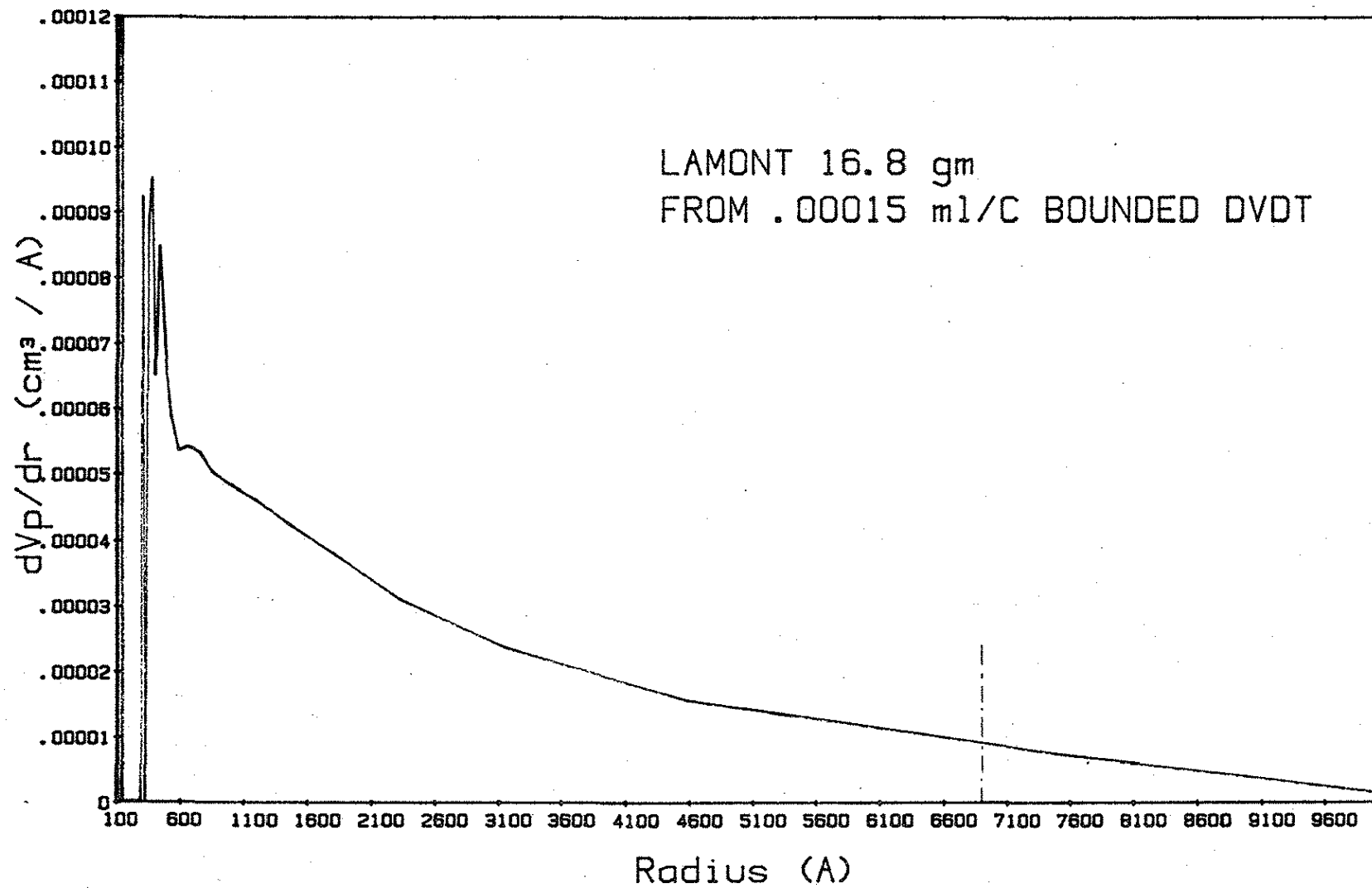


Figure 18. Pore (body) size distribution of Lamont,
(mercury intrusion median pore size by W. Dubberke).

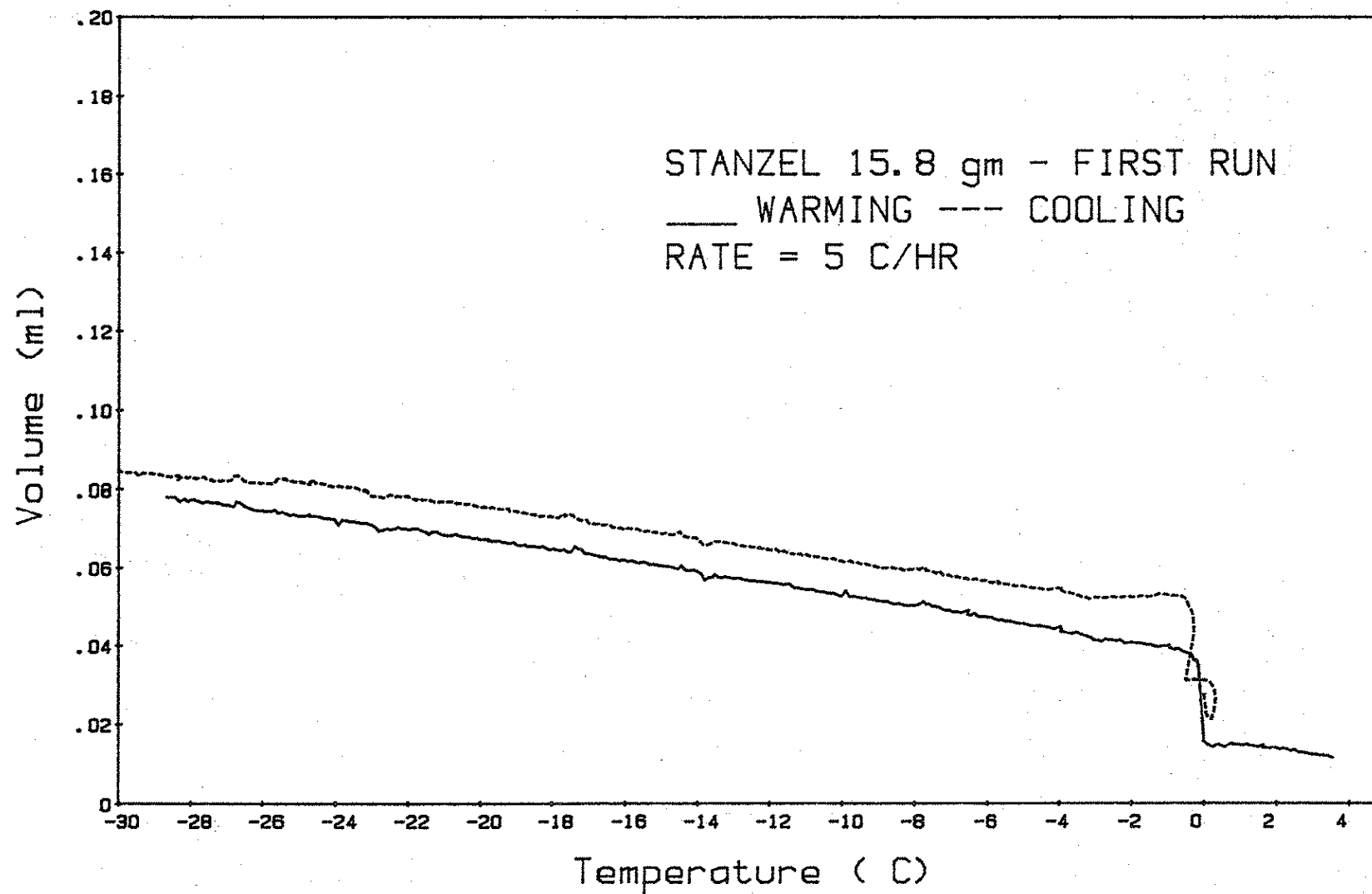


Figure 19. Ice porosimetry of Stanzel (Bed 15A), first run.

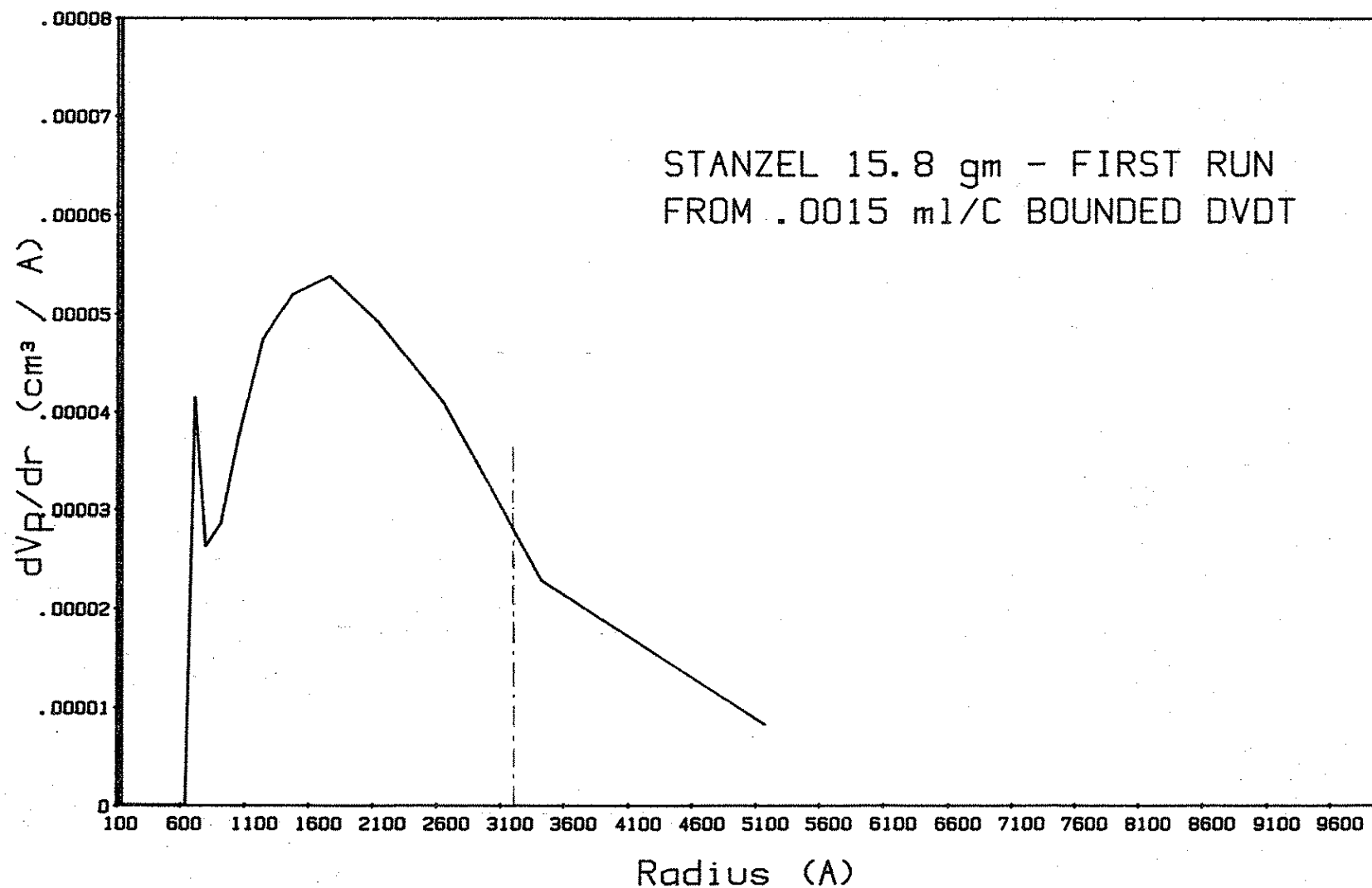


Figure 20. Pore (body) size distribution of Stanzel (Bed 15A) by ice porosimetry,
first run (mercury intrusion median pore size by W. Dubberke).

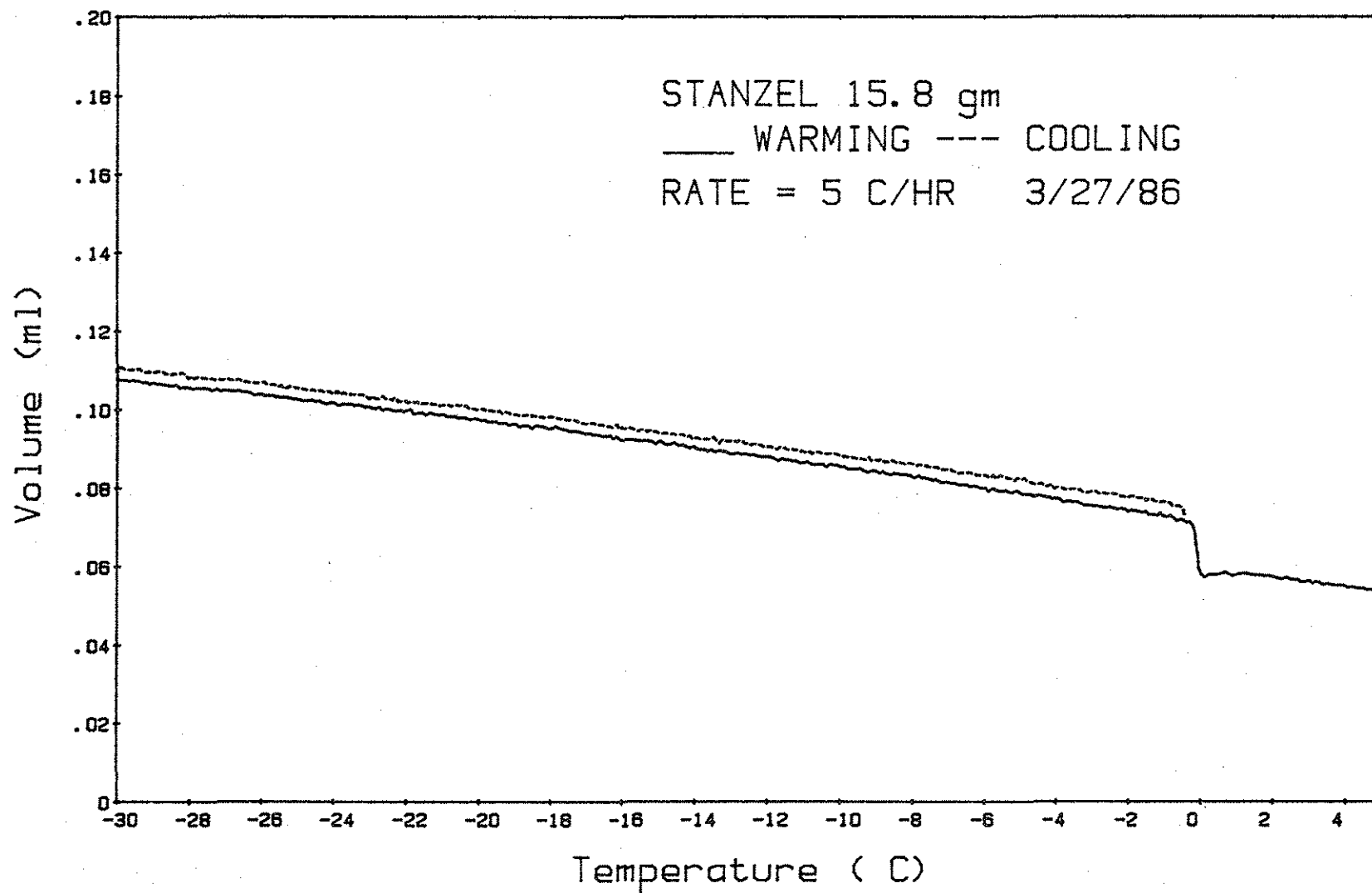


Figure 21. Ice porosimetry of Stanzel (Bed 15A), second run.

(Note absence of periodic noise seen in preceding plots, achieved by progressive improvement of the hardware.)

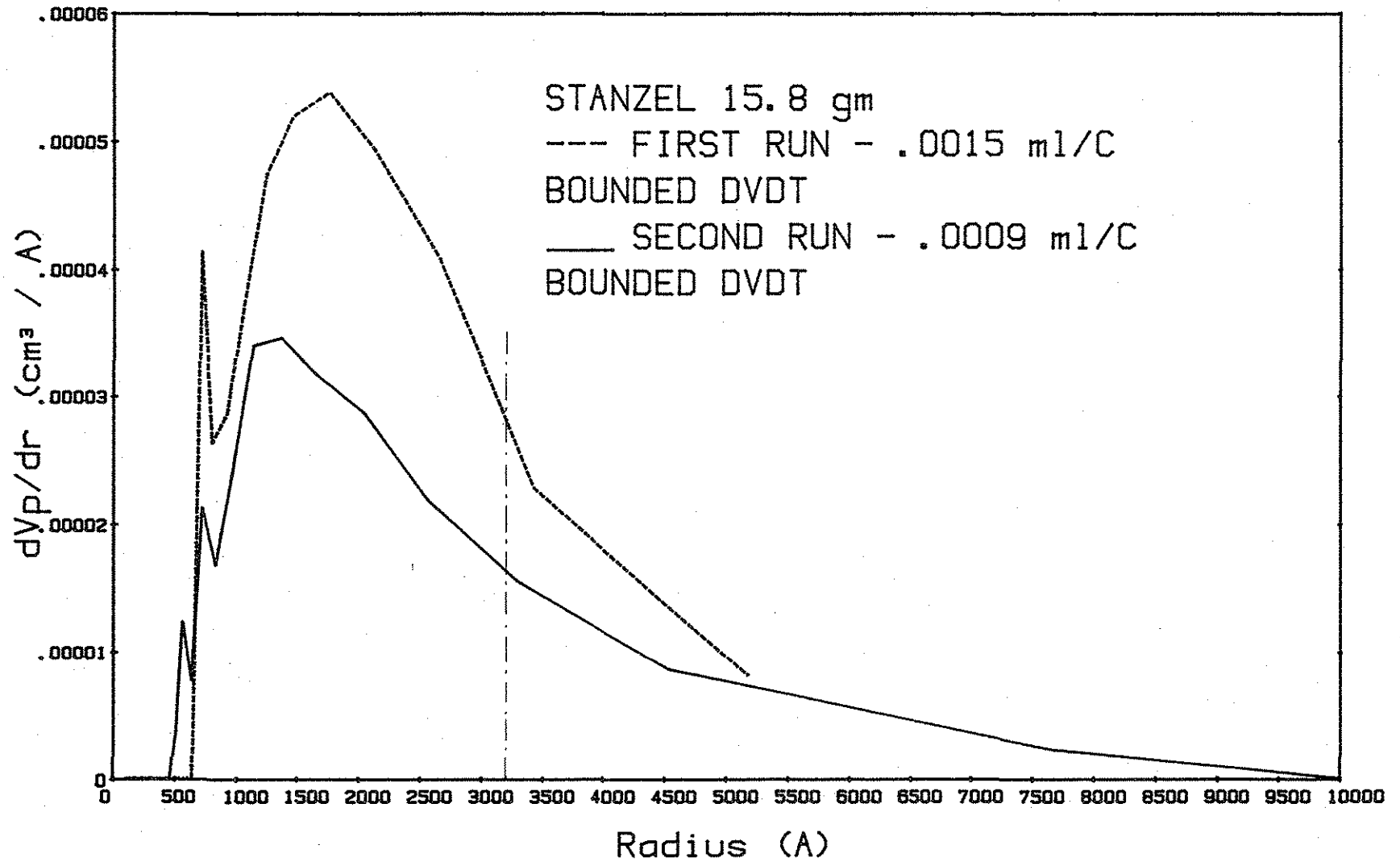
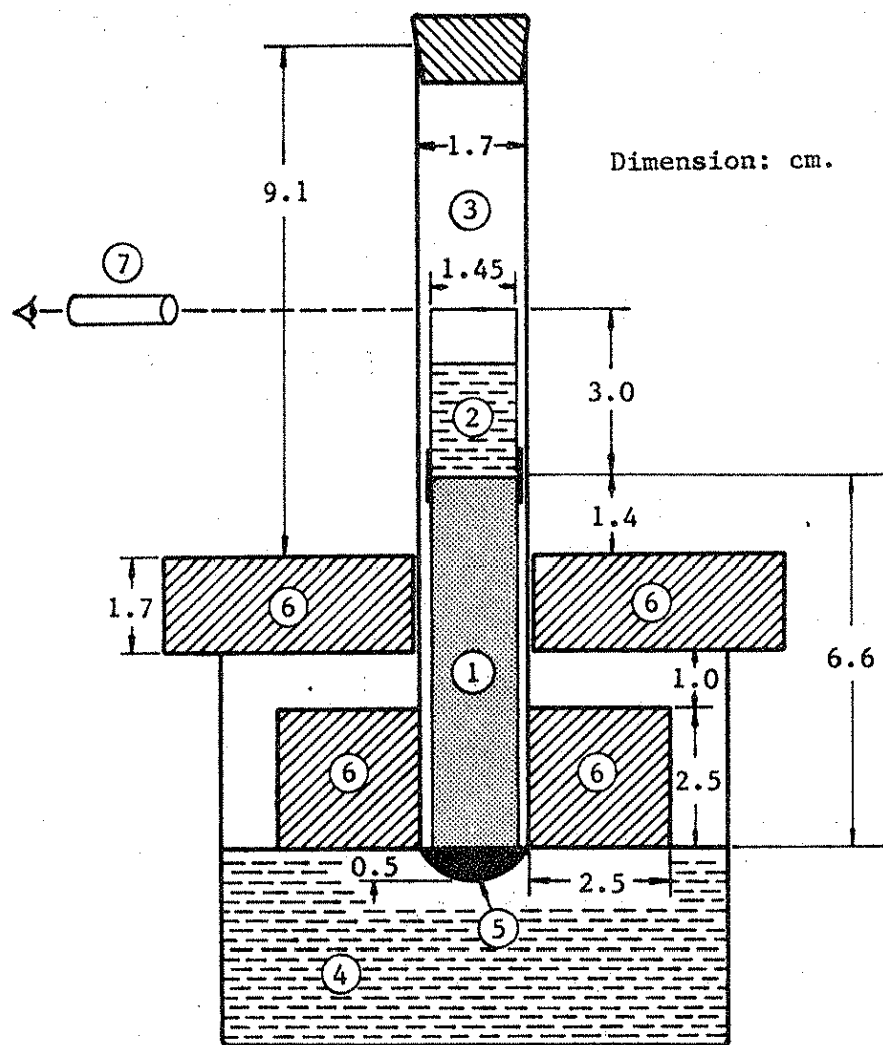


Figure 22. Pore (body) size distribution of Stanzel (Bed 15A)
 from first and second runs of ice porosimetry,
 (mercury intrusion median pore size by W. Dubberke).



- Legend: (1)--Porous sample (5)--Bulk ice
 (2)--Water reservoir (6)--Styrofoam insulation
 (3)--Glass tube (guide) (7)--Cathetometer
 (4)--Cryostat coolant

Figure 23. Apparatus for determination of the rate of ice growth.

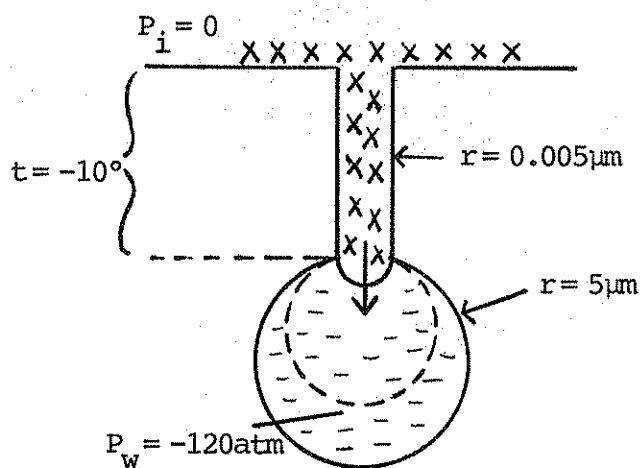


Fig. 24 (a)

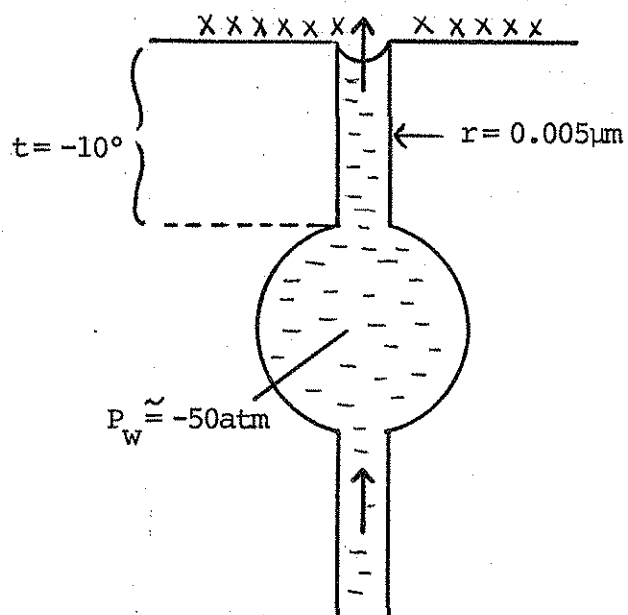


Fig. 24 (b)

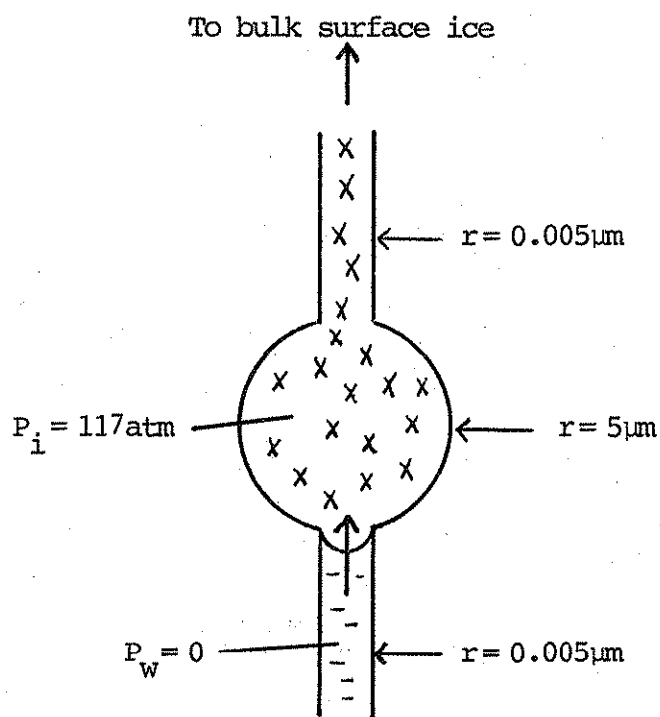


Fig. 24 (c)

Figure 24. Illustrations of possible freezing phenomena in water filled spherical pores.

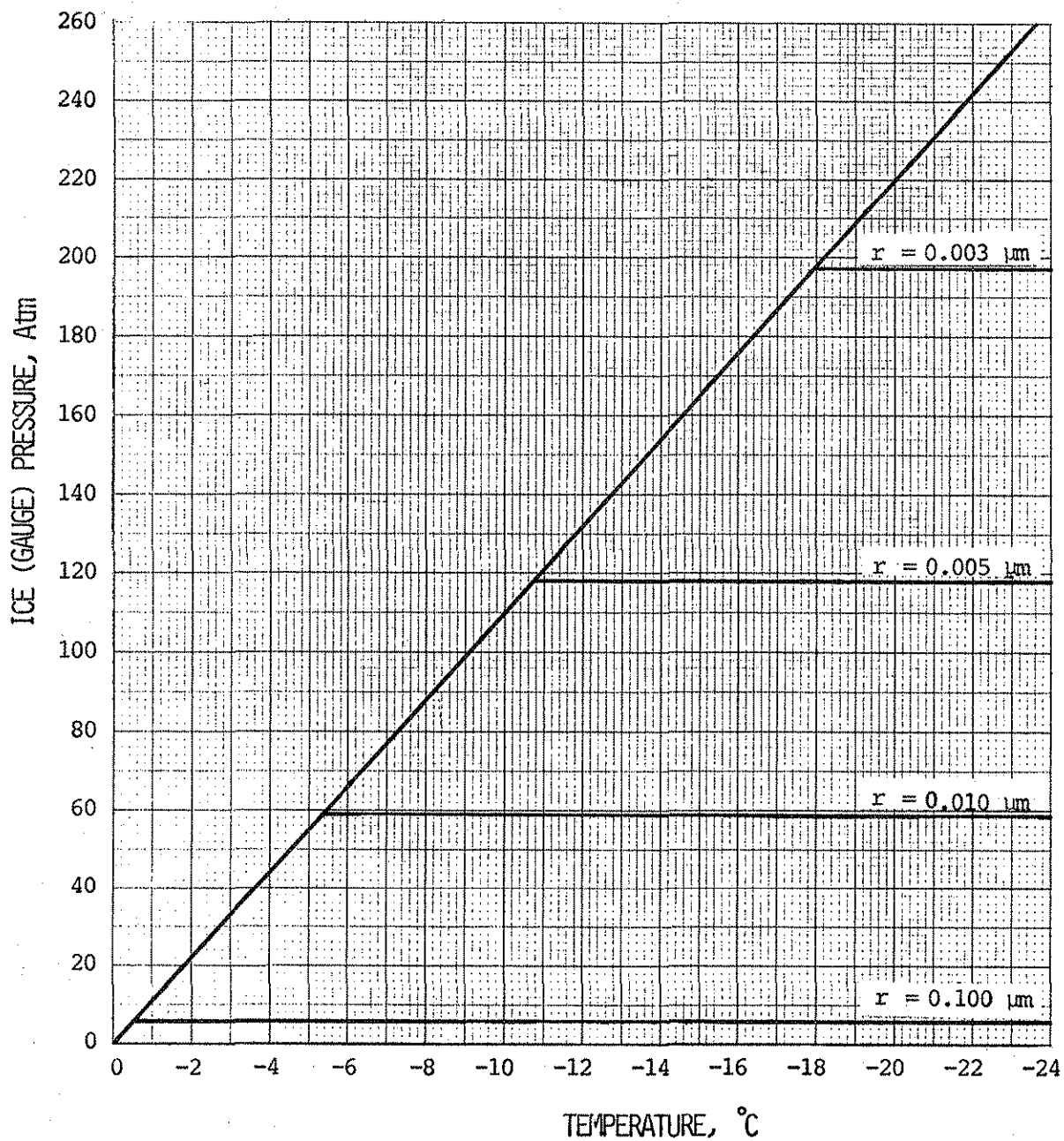


Figure 25. Ice pressure chart.

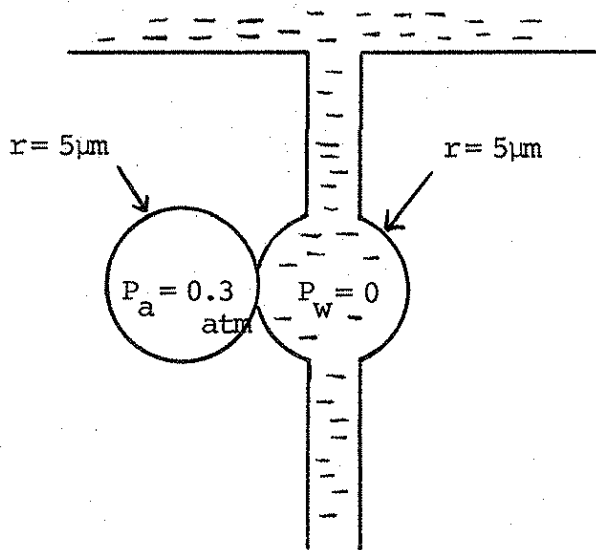


Fig. 26 (d)

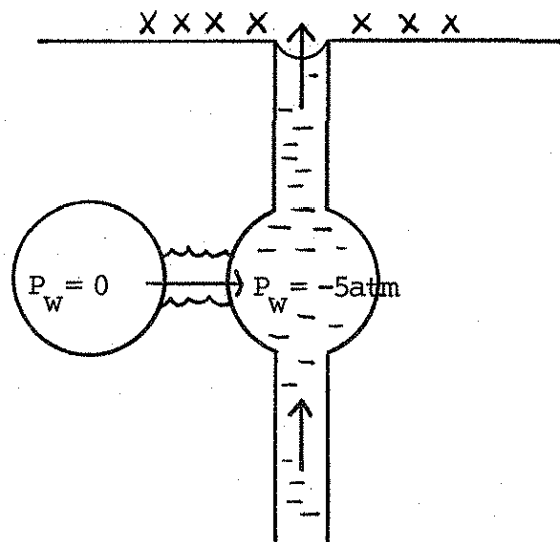


Fig. 26 (e)

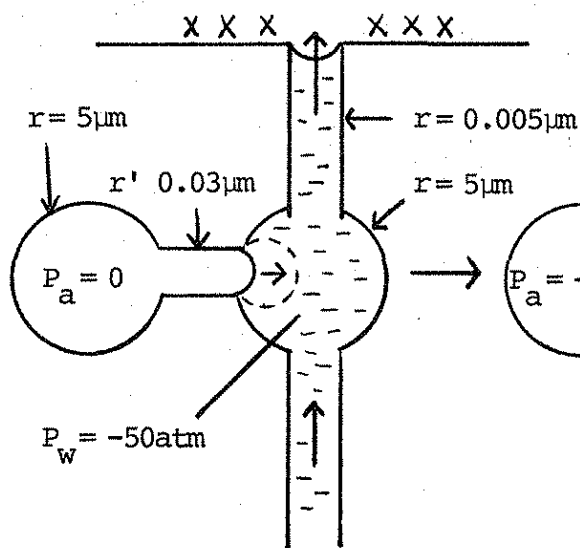


Fig. 26 (a)

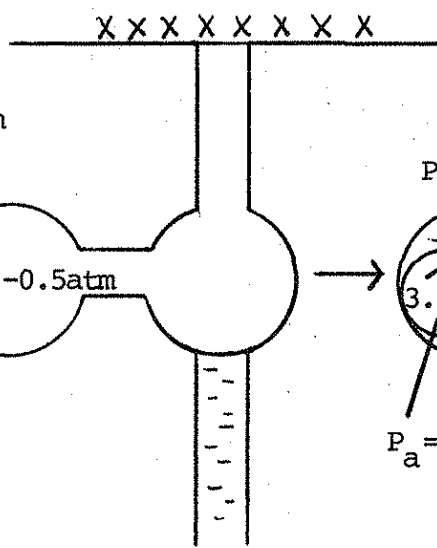


Fig. 26 (b)

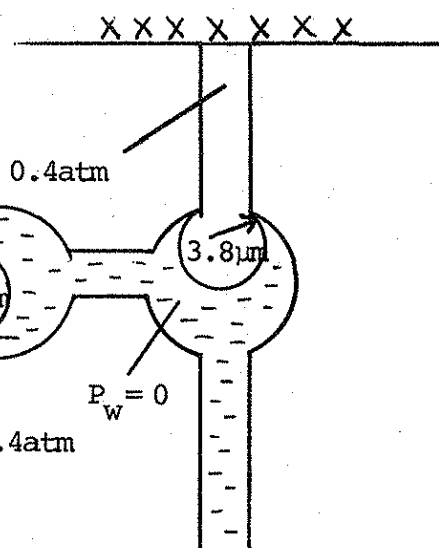


Fig. 26 (c)

Figure 26. Illustration of the consequence of connecting an air pocket to a water filled spherical cavity.

APPENDIX I

PHASE TRANSITION POROSIMETRY

B. V. Enüstün, J. Eckrich and T. Demirel
Department of Civil Engineering,
Iowa State University, Ames, Iowa

Presented to International Symposium-Workshop on Particulate and Multi-Phase Processes and 16th Annual Meeting of the Fine Particle Society, 22-26 April 1985, Miami Beach, Florida.

ABSTRACT

An experimental method was developed to determine pore size distribution and other porosimetric properties of microporous materials. It is based on phase transition temperatures of pore water in porous materials. Phase transitions are detected by a computerized dilatometric method.

Experimental results obtained with Vycor porous glass show that the method is superior to mercury porosimetry, as it is free of such problems as uncertainties associated with the contact angle and entrapment of mercury.

PHASE TRANSITION POROSIMETRY

B. V. Enüstün*, J. Eckrich and T. Demirel
Department of Civil Engineering
Iowa State University, Ames, Iowa 50011 U.S.A.

1. INTRODUCTION

In addition to direct microscopy, the available indirect methods of pore size estimations of porous materials are the capillary condensation of a vapor and the mercury porosimetry.

The capillary condensation method makes use of the well known Kelvin equation. It is an elaborate and time consuming method. Also, there are evidences for occasional failure of the Kelvin equation.^{1,2} This failure was discussed by one of us elsewhere.³

The intrusion-extrusion hysteresis invariably observed in mercury porosimetry is attributed to the advancing-receding hysteresis in the mercury/ matrix contact angle and the pore structure. The ambiguity in relative contributions of these two effects is an extensively commented and discussed uncertainty in mercury porosimetry. The most recent contribution to this subject is a publication by Conner et al⁴, who have shown that it is the extrusion pressure which is related to the actual size of the pore body. A serious uncertainty, however, lies in the entrapment of mercury during extrusion. Making the erroneous assumption that the extruded pore volume, in spite of entrapment, is representative of the entire pore structure of the sample, it is not possible to obtain the correct pore size distribution.

Another method of estimating pore size distribution as suggested by various authors and used by Brun et al⁵ is based on solid/liquid phase transition in capillaries. The latter authors related thermodynamically the capillary freezing point to the pore size assuming the validity of the homogeneous nucleation model and persistence of a liquid film in the capillaries upon freezing. By a calorimetric method, they followed freezing of liquids such as water and benzene present in the capillaries of various microporous materials at saturated state.

However, as discussed by one of us previously⁶, freezing by homogeneous nucleation is a rate process which may be treated along the lines of the Volmer theory⁷ and not by pure thermodynamics. Besides, we have recently showed that at least in the presence of bulk ice surrounding a saturated sample capillary freezing takes place in accordance with the plastic ice theory due to Everett

*Visiting Professor on leave from Department of Chemistry, Bogazici University, Istanbul, Turkey

et al^{8,9}, i.e. initiated not by in situ nucleation, but by the bulk ice, as will be reported elsewhere.

In this paper we present a similar method of porosimetry based on solid \leftrightarrow liquid phase transition of pore water. It differs, however, from the method proposed by Brun et al in interpreting and evaluating the experimental results, as it is based on the plastic ice model instead of in situ nucleation, making no allowance for presence of a liquid film upon freezing. Another difference is that phase transitions are followed by dilatometric measurements.

2. CAPILLARY FREEZING AND MELTING

Assuming that the pore geometry of the sample can be represented by randomly intersecting spheres or cylindrical capillaries with or without constrictions, it can be shown, using the plastic ice model, that the solid \leftrightarrow liquid phase transition of water in a capillary of a saturated porous material takes place at a temperature t C given by

$$t = -2\gamma T_0 / \rho \lambda r \quad (1)$$

where T_0 is the normal melting point of ice in K, λ is the heat of fusion of ice per unit mass, ρ is the density of water, γ is the ice/water interfacial tension at t , and r is the effective pore radius. In solid \rightarrow liquid transition the effective radius is the radius of the actual pore body, while in liquid \rightarrow solid transition it is the radius of the constriction at the opening of the pore body concerned. Working with porous Vycor glass of known pore size distribution established by electron microscopy, it was shown that Eq. 1 is accurately applicable to solid \rightarrow liquid transition, using independently estimated values of γ .¹⁰

The thermodynamic treatment of capillary phase transition by Brun et al⁵ is essentially the same as the one used in the derivation of Eq. 1 previously. However, their interpretation that the freezing point but not the melting point is related to the pore size disagrees with our treatment and findings.

3. DILATOMETRIC PHASE TRANSITION POROSIMETRY

3.1 Principles

Derivation of pore size distribution through solid \leftrightarrow liquid phase transition requires experimental data on the volume of water undergoing phase transition as a function of temperature. Eliminating temperature between this correlation and Eq. 1 the volume distribution of pore size can be obtained. The experimental method to provide the former correlation may be based on measurement of any physical property which is proportional to the quantity of water going through phase transition. It has been found previously¹⁰ that the measurement of volume change of a porous sample saturated with water during freezing cycle can be used for this purpose. Preliminary experiments with porous Vycor glass carried out recently in our laboratory showed that the magnitude of volume increase upon freezing equalled the volume decrease observed upon rewarming, within the experimental error. The observed volume changes correspond to the extrusion of excess volume of ice out of the pores and to the penetration of bulk ice into the pores during the freezing and melting cycles, respectively.

3.2 Pore Size Distribution

Consider that a porous material saturated with water is placed in a mercury dilatometer, frozen in a cryostat and allowed to rewarm gradually. According to Eq. 1 melting starts at a temperature t_1 in the smallest pores and ends at t_2 in the largest pores. Let V_s be the bulk volume of the saturated sample and V_i the volume of excess ice extruded from the pores and V_m the total volume of mercury in the dilatometer, V_d the capacity (volume) of the dilatometer immersed in the cryostat at temperature t , and V the volume of mercury in the dilatometer stem at room temperature. Then,

$$V_m + V_s + V_i = V_d + V \quad (2)$$

or

$$dV/dt = dV_m/dt + dV_s/dt - dV_d/dt + dV_i/dt \quad (3).$$

The sum of the first three terms in the right hand side of Eq. 3 is a temperature independent positive constant, a , i.e.

$$dV_m/dt + dV_s/dt - dV_d/dt = a \quad (4).$$

From (3) and (4),

$$dV/dt = a + dV_i/dt \quad (5).$$

If no phase change takes place over a temperature range, $dV_i/dt = 0$, $dV/dt = a$, i.e., V varies linearly with t with a slope of a . Any deviation from this linearity indicates and measures the phase change. In such a case, since $dV_i/dt < 0$, the slope will be less than a .

Let V_p be the pore volume of the sample. An increment of pore volume dV_p in which ice is transformed into liquid water is given by

$$dV_p = -dV_i/\phi \quad (6)$$

where ϕ is the fractional volume change due to freezing of water at temperature t , i.e.

$$\phi = (\text{vol. of ice} - \text{vol. of water})/\text{vol. of water} \quad (7).$$

From Eq. 5 and Eq. 6 we have

$$dV_p/dt = (a - dV/dt)/\phi \quad (8).$$

Finally, from Eq. 8 pore size distribution can be expressed as

$$dV_p/dr = (a - dV/dt)(dt/dr)/\phi \quad (9).$$

The term dt/dr can be obtained from Eq. 1, considering that γ depends significantly on temperature¹⁰ as

$$\gamma = \gamma_0 + 2.5 \times 10^{-4} t \quad (10)$$

where the constant 2.5×10^{-4} is a dimensional constant for use with S.I. units, γ_0 is the value of γ at 0 C. Combining Eq. 10 and Eq. 1, one gets

$$r = (-2\gamma_0/t - 5 \times 10^{-4}) T_0/\rho\lambda \quad (11)$$

and

$$dt/dr = \rho \lambda t^2 / 2 \gamma_o T_o \quad (12).$$

Substituting Eq. 12 into Eq. 9 we obtain

$$dV_p/dr = (a - dV/dt) \rho \lambda t^2 / 2 \gamma_o T_o \phi \quad (13).$$

From the experimental V versus t data, size distribution curve can be constructed by computing dV_p/dr values from Eq. 13 and plotting against corresponding r values from Eq. 11. The constant a can be estimated in each case from the slope of V versus t plot at temperatures above 0 C.

3.3 Constriction Size Distribution

As already mentioned, the liquid-solid transition point is related to the radius of pore constrictions by Eq. 1 or more explicitly Eq. 11. Therefore, Eq. 13 can also be used to determine the constriction size distribution from V versus t data obtained during cooling cycle.

3.4 Pore Volume

The pore volume V_p of the sample is obtained by integrating either the pore size distribution or constriction size distribution over the entire size range, viz.

$$V_p = \int_{r_1}^{r_2} (dV_p/dr) dr \quad (14).$$

Comparison of the volumes V_p obtained from pore size and constriction size distribution using Eq. 14 gives the opportunity for checking the validity of the method and the internal consistency of the experimental results. This should also be evident from closing of the hysteresis loop.

3.5 Pore Surface

Assuming that a pore body has a cylindrical geometry with a radius r, the total pore surface area A is calculable by

$$A = 2 \int_{r_1}^{r_2} (1/r) (dV_p/dr) dr \quad (15).$$

It can be shown that in the case of spherical pores with small enough inter-connecting necks the factor 2 in the right hand side of Eq. 15 becomes 3. It may be suggested that a constant of 2.5 instead of 2 should be used as an approximation in Eq. 15 to represent an irregularly shaped pore geometry.

4. EXPERIMENTAL METHOD

The dilatometer used is shown in Fig. 1. Its total capacity is 35 cm³. It was made of Pyrex and consisted of a cylindrical cup and an upper attachment which carried a 20 cm long graduated and calibrated capillary stem of 0.1 cm³ capacity, a capillary mercury inlet equipped with a stopcock and a 10 cm³ reservoir, a dead-end inlet to house a thermistor, and a sealed tungsten contact wire. The attachment fitted into the cup by a 29/42 ground joint. A 22 cm long aluminum tubing sheath slipped snugly over the capillary stem functions as the outer member of a cylindrical capacitor.

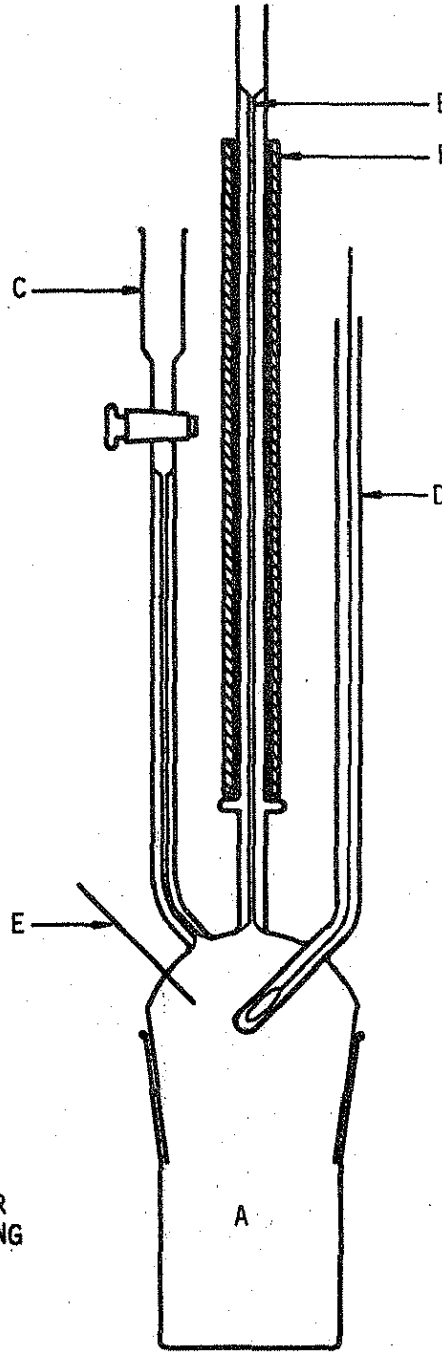
- 
- A - CUP
 - B - CAPILLARY STEM
 - C - MERCURY RESERVOIR
 - D - THERMISTOR HOUSING
 - E - TUNGSTEN WIRE
 - F - ALUMINUM SHEATH

Fig. 1. Dilatometer

The cryostat used is a HAAKE A82 suitable to maintain constant temperatures above -40°C within $\pm 0.01^{\circ}\text{C}$.

The porous sample to be studied is saturated with water by a suitable method such as capillary suction, vacuum saturation, steam saturation, etc. and placed in the dilatometer cup. At that stage it must be visibly wet and surrounded by a film of excess liquid. Powdered samples may be introduced into the dilatometer in the form of pastes enclosed in suitable containers. The dilatometer is assembled and filled with mercury through the inlet so that the mercury level reaches the upper end of the stem. The assembly is immersed in the cryostat maintained at a few degrees above 0°C up to the lower end of the stem. When the thermal equilibrium is established, the mercury level is reset and the aluminum sheath is slipped over the stem. The cryostat temperature is lowered at a rate of 5 to 10°C/hr to about -35°C . Subsequently, it is raised again with the same rate to about $+4^{\circ}\text{C}$.

While the thermistor signals the temperature of the dilatometer, the capacitance of the above mentioned condenser consisting of the aluminum sheath and the mercury thread in the stem, measures the volume V . These data are simultaneously supplied to an Apple IIe Personal computer through respective interfaces.

The software automatically controls the bath temperature and records one set of V versus t data every 20 seconds throughout a cooling-rewarming cycle. The accumulated data are saved on a magnetic disc.

First dV/dt versus t curve is computed from these data. dV_p/dr versus r is obtained using Eq. 13 in conjunction with Eq. 11 for subsequent output to a Hewlett-Packard HP-7220 X-Y plotter, or to the Apple's screen. Finally, V_p and A can be calculated by Eq. 14 and Eq. 15, respectively.

5. RESULTS AND DISCUSSION

After necessary calibrations of the instrument, the method mentioned above was used to explore porosimetric properties of porous Vycor glass on which some previously obtained data were available. Fig. 2 is a computer plot of volume versus temperature curve of phase transition porosimetry obtained for a 5.55 cm^3 sample of porous Vycor glass. The extreme, linear sections of this plot with positive slopes indicate absence of phase transition, while the middle curved sections joining the linear sections correspond to capillary freezing and melting. Two features of this plot are noteworthy:

(a) Freezing and melting signals are large enough for accurate analysis of size distributions.

(b) The hysteresis loop practically closes at the end of the cycle.

The significance of the latter feature is better understood when this plot is compared with Fig. 3 which is a mercury porosimetric intrusion-extrusion plot obtained with the same sample indicating that half of the mercury introduced is entrapped in the pores upon attempted extrusion, as already mentioned in Sec. 1. In the present method such an entrapment (of ice) is physically out of the question. Fig. 2 reveals the superiority of this method to mercury porosimetry in this respect.

Figure 4 shows the size distribution curves computed from the phase transition V vs t data given in Fig. 2, while Fig. 5 shows mercury porosimetric dV_p/dr curves. While the mercury intrusion peak at 25 \AA radius (modal constriction radius) in Fig. 5 is in good agreement with the freezing peak at 21 \AA radius in Fig. 4, the extrusion peak (modal pore body radius) at 80 \AA disagrees significantly with the melting peak at 42 \AA . This disagreement shows that

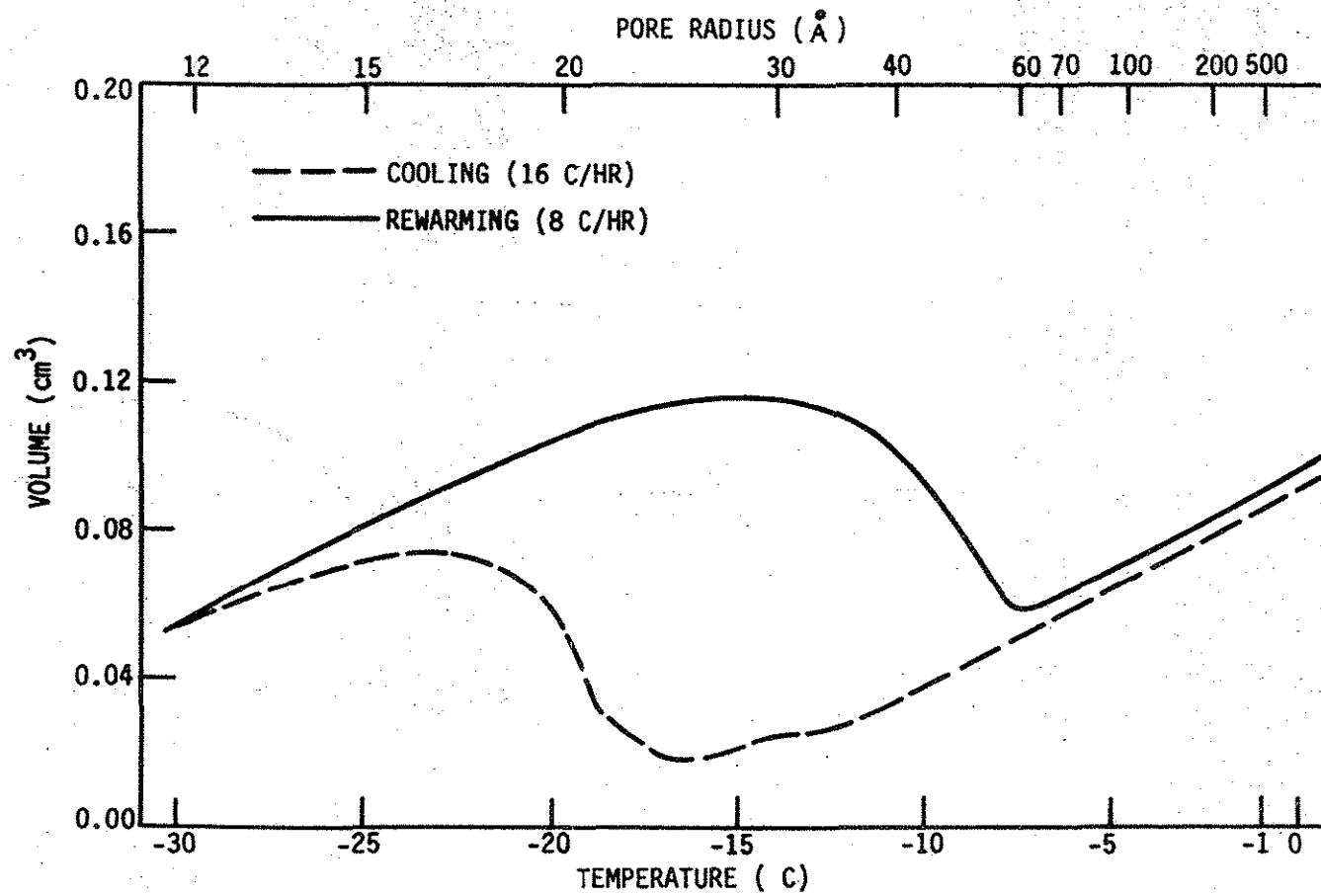


FIGURE 2. Phase transition porosimetry of Vycor (5.55 cm³)

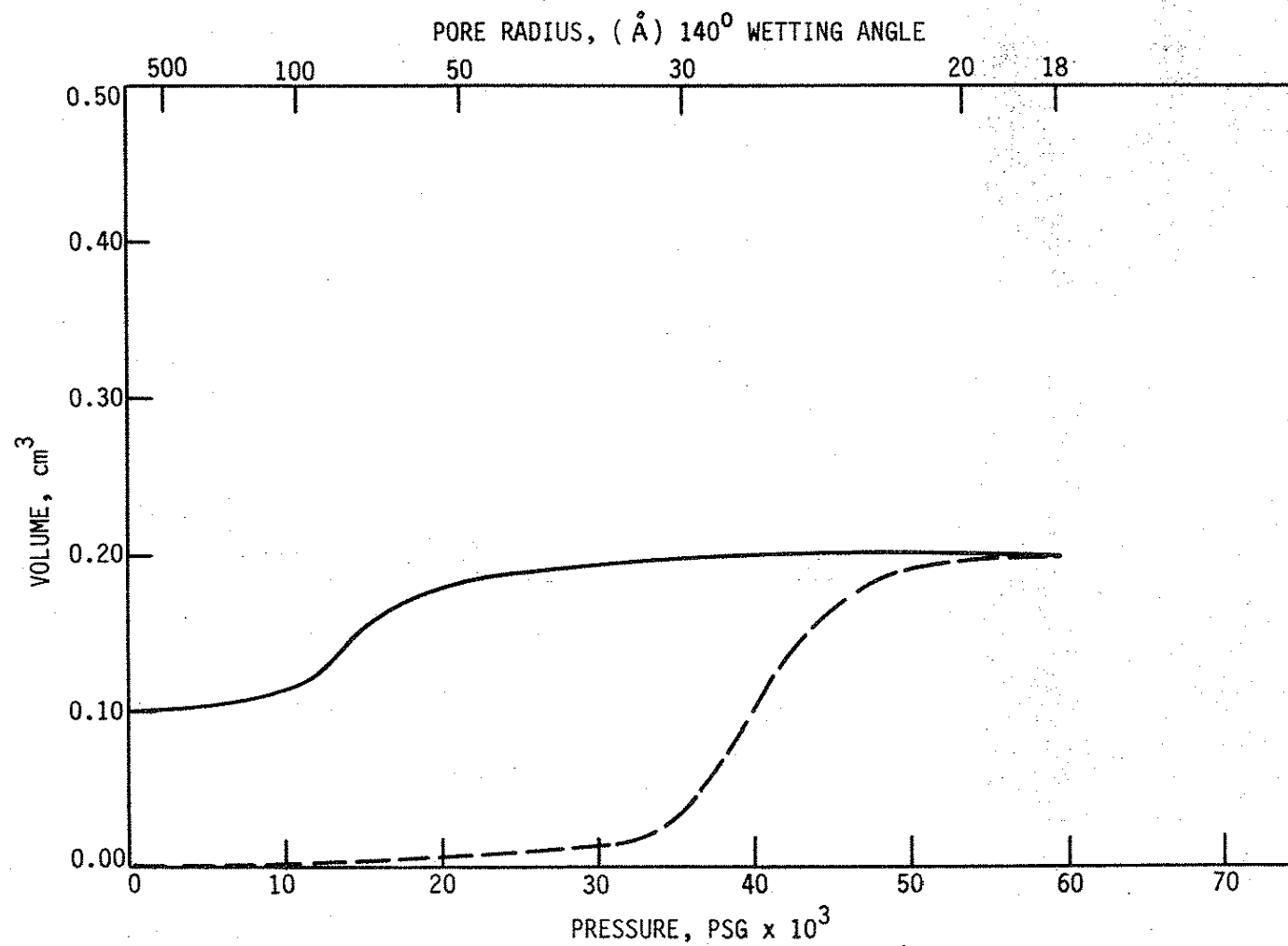


FIGURE 3. Mercury porosimetry of Vycor (0.67 cm³): V_p plotted vs. pressure and pore radius for intrusion (----) and extrusion (—). (1 PSI = 6894.8 Nm⁻²)

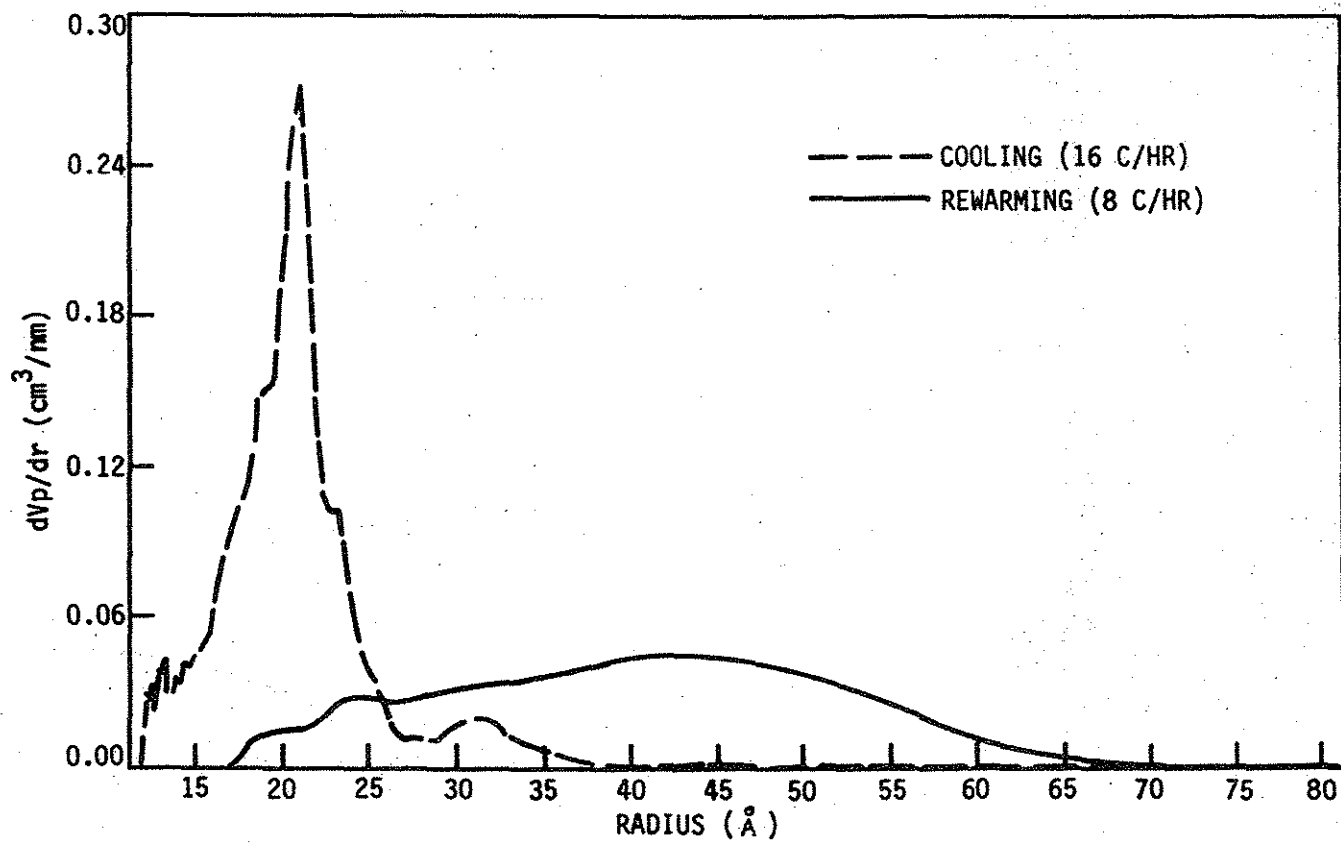


FIGURE 4. Pore body size (—) and pore neck size (---) distribution of Vycor (5.55 cm^3) by phase transition porosimetry.

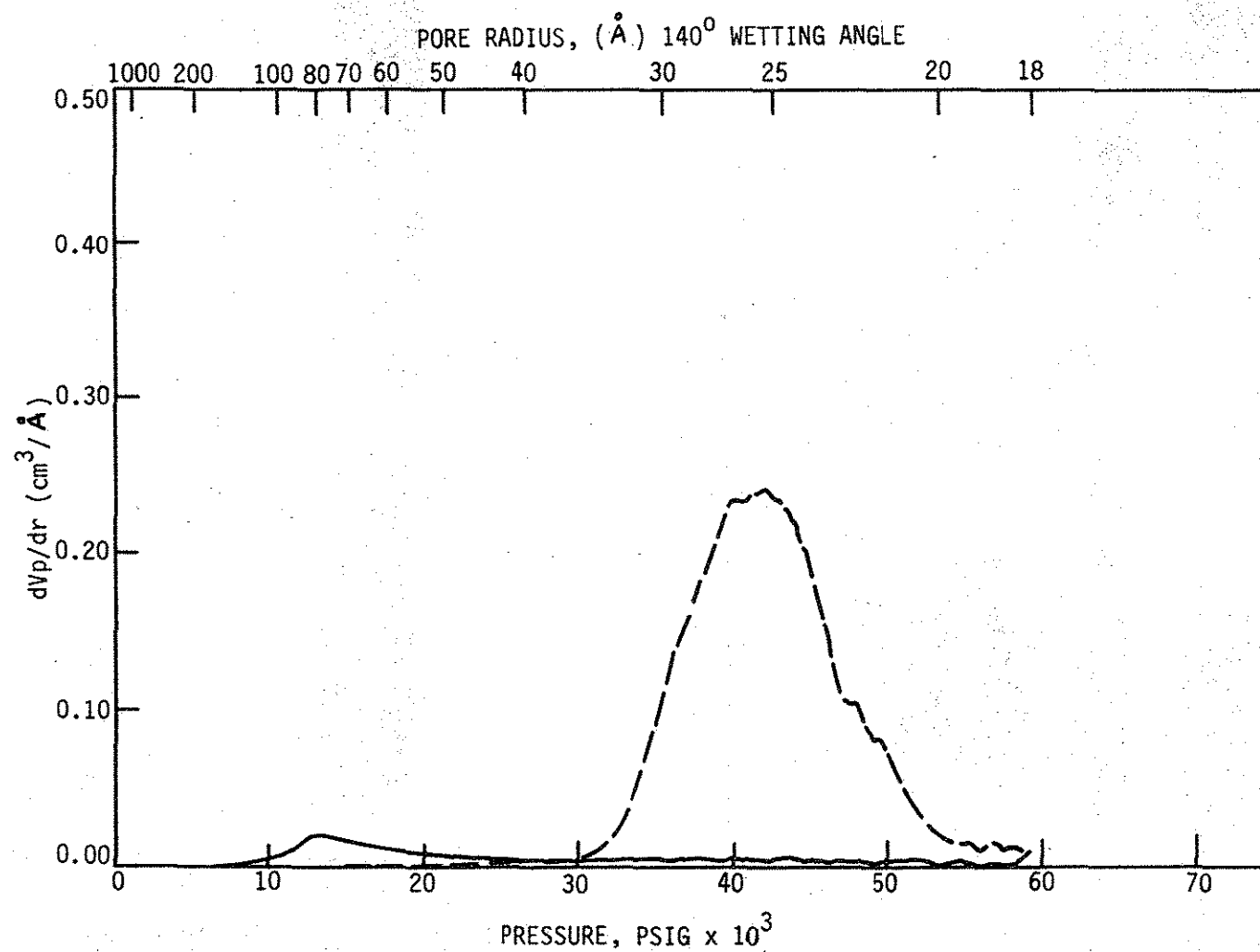


FIGURE 5. Mercury porosimetry of Vycor (0.67 cm^3): dV_p/dr plotted vs. pressure and pore radius for intrusion (----) and extrusion (—). (1 PSI = 6894.8 Nm^{-2})

mercury can be extruded only from the larger pores and, therefore, as far as pore size distribution is concerned the extruded volume does not represent the entire sample as discussed in Sec. 1.

Some characteristic porosimetric data obtained using various methods with porous Vycor glass are tabulated in Table 1.

The numerical values of various constants used in above computations were as follows: $\gamma_0 = 29 \times 10^{-3} \text{ Nm}^{-1}$, $T_0 = 273.16 \text{ K}$, $\rho = 1.000 \text{ g cm}^{-3}$, $\lambda = 333.3 \text{ J g}^{-1}$. The value of ϕ was calculated at each temperature from the relevant data available in standard handbooks.

6. SUMMARY AND CONCLUSION

An experimental method was developed to determine pore size distribution and other porosimetric properties of microporous materials. It is based on phase transition temperatures of pore water in porous materials. Phase transitions are detected by a computerized dilatometric method.

Experimental results obtained with Vycor porous glass show that the method is superior to mercury porosimetry, as it is free of such problems as uncertainties associated with the contact angle and entrapment of mercury.

7. ACKNOWLEDGMENTS

We gratefully acknowledge that this study is a part of a research project funded by the Iowa Department of Transportation, Highway Division and Iowa Highway Research Board. We also extend our gratitude to the NATO Scientific Affairs Division and the Bogazici University for their partial support granted to one of us.

The results and conclusions presented in this paper reflect the opinion of the authors alone, and not necessarily those of the above mentioned institutions.

8. REFERENCES

1. Shereshefsky, J. L. and Carter, C. P., J. Am. Chem. Soc., 72, 3682 (1950).
2. Folman, M. and Shereshefsky, J. L., J. Phys. Chem., 59, 607 (1955).
3. Enüstün, B. V., Bogazici University J., (Chem.), 8-9, 9 (1980-81).
4. Conner, W. C., Lane, A. M., and Hoffman, A. J., J. Colloid Interface Sci., 100, 185 (1984).
5. Brun, M., Lallemend, A., Quinson, J. F., and Eyraud, C., Thermochimica Acta, 21, 59 (1977).
6. Enüstün, B. V., Sentürk, H. S., and Koksai, K., RILEM/CIB Symposium, Moisture Problems in Buildings, Helsinki, 1965, Report 2-13.
7. Hesstvedt, E., Norges Geotekniske Inst. No. 56, 7 (1964).
8. Everett, D. H., Trans. Faraday Soc., 57, 1541 (1961).

TABLE 1. Pore size range, porosity and specific surface of porous Vycor glass obtained using various methods.

Method	Range of pore body radius, Å			Range of pore neck radius, Å			Porosity % by vol.	Specific surface, m ² /g
	Min.	Mode	Max.	Min.	Mode	Max.		
Phase trans. poros.*	17	42	75-100	12	21	40	25 ^a -27 ^b	135 ^c
Mercury poros.*	19	80	-	18	25	35	29 ^d	-
Conductance**	17	36	60	-	24	26	-	-
TEM ¹¹	15	38 ^e	85	-	-	-	-	-
Manufacturer's specification	10	-	100	-	-	-	28	150-200

* This study.

** This study, by previously developed method^{6,10} of electrical conductance.

^a From rewarming data.

^b From cooling data.

^c Assuming spherical pores.

^d From intrusion.

^e After converting number-size distribution to volume-size distribution.

9. Everett, D. H., and Haynes, J. M., RILEM Bull., 27, 31 (1965).
10. Enüstün, B. V., Sentürk, H. S., and Yurdakul, O., J. Colloid Interface Sci., 65, 509 (1978).
11. Enüstün, B. V., and Enuysal, M., METU, J. Pure & Appl. Sci. 3, 81 (1970).